



U-Pb SHRIMP Zircon Ages, Geochemical and Sr-Nd Isotopic Compositions of the Late Cretaceous I-type Sarıosman Pluton, Eastern Pontides, NE Turkey

ABDULLAH KAYGUSUZ¹, BIN CHEN², ZAFER ASLAN³,
WOLFGANG SIEBEL⁴ & CÜNEYT ŞEN⁵

¹ Department of Geological Engineering, Gümüşhane University, TR-29000 Gümüşhane, Turkey
(E-mail: abdullah@ktu.edu.tr)

² Department of Geological Engineering, Peking University, Beijing 100871, China

³ Department of Geological Engineering, Balıkesir University, TR-10145 Balıkesir, Turkey

⁴ Institute of Geosciences, Universität Tübingen, Wilhelmstr. 56, D-72074 Tübingen, Germany

⁵ Department of Geological Engineering, Karadeniz Technical University, TR-61080 Trabzon, Turkey

Received 03 June 2008; revised typescript received 13 January 2009; accepted 21 April 2009

Abstract: The petrogenesis and U-Pb SHRIMP zircon ages of the Late Cretaceous Sarıosman pluton in the Eastern Pontides is investigated by means of whole-rock Sr-Nd isotope data with field, petrographic and whole-rock geochemical studies. The bulk of the I-type Sarıosman pluton consists of biotite-hornblende monzogranite, with minor quantities of porphyritic hornblende-biotite monzogranite. The biotite-hornblende monzogranite contains a number of mafic microgranular enclaves (MMEs) of quartz monzodiorite composition. U-Pb zircon sensitive high-resolution ion microprobe dating (SHRIMP) dates the magma emplacement age of the biotite-hornblende monzogranite at 82.7 ± 1.5 Ma. The rocks of the pluton show high-K calc-alkaline, metaluminous to slightly peraluminous characteristics, and are enriched in large ion lithophile elements (LILE) and light rare earth elements (LREE) relative to high field strength elements (HFSE), thus displaying features of arc-related granitoids. Chondrite-normalised rare earth-element (REE) patterns have concave upward shapes ($\text{La}_{\text{cn}}/\text{Lu}_{\text{cn}} = 10.1-17.4$) with pronounced negative Eu anomalies ($\text{Eu}/\text{Eu}^* = 0.61-0.80$). Initial ϵ_{Nd} values vary between -3.0 and -4.1 and initial $^{87}\text{Sr}/^{86}\text{Sr}$ values between 0.7062 and 0.707. The MMEs are characterised by higher Mg-numbers (27–29) and lower values of both SiO_2 (56–58 wt%) and aluminium saturation index (0.9–1.0), compared to the monzogranites. Fractionation of plagioclase, hornblende and Fe-Ti oxides played an important role in the evolution of the Sarıosman pluton. The crystallisation temperatures of the melts ranged from 700 to 800 °C and a relatively shallow intrusion depth (~2 to 7 km) is estimated from the Al-in-hornblende geobarometry. The geochemical and isotopic compositions of the Sarıosman pluton suggest an origin through dehydration melting of mafic lower crustal source rocks.

Key Words: SHRIMP dating, Sarıosman pluton, mineral chemistry, I-type, Sr-Nd isotope geochemistry, eastern Pontides

Üst Kretase Yaşılı I-Tipi Sarıosman Plutonu'nun U-Pb SHRIMP Zirkon Yaşları, Jeokimyasal ve Sr-Nd İzotopik Bileşimleri, Doğu Pontidler, Kuzeydoğu Türkiye

Özet: Doğu Pontidler'de Geç Kretase yaşılı Sarıosman plutonu'nun petrojenezi ve U-Pb SHRIMP zirkon yaşları, tüm kayaç Sr-Nd izotop verileri ve arazi, petrografik ve tüm kayaç jeokimyasal verilerine dayanarak irdelenmiştir. I-tipi Sarıosman plutonu'nun ana kütlesi biyotit-hornblend monzogranit ve daha az olarak da porfirik hornblend-biyotit monzogranitinden oluşur. Biyotit hornblend monzogranitler az sayıda kuvarslı monzodiorit bileşimli mafik magmatik anklavlardır. U-Pb zirkon SHRIMP yöntemine göre biyotit hornblend monzograniti oluşturan magmanın yerlesim yaşı 82.7 ± 1.5 My'dır. Plutonu oluşturan kayaçlar yüksek K'lu kalk alkalen, metalümin kışmen de peralümin karaktere sahiptirler. Kayaçlar yüksek alan enerjili elementlere kıyasla büyük iyon yarıçaplı litofil elementler ve hafif nadir toprak elementlerce zenginleşmiş olup, yay ile ilişkili granitoyid özelliği gösterirler. Kondirite göre

normalleştirilmiş nadir toprak element dağılımları konkav şekilli ($\text{La}_{\text{cn}}/\text{Lu}_{\text{cn}} = 10.1\text{--}13.4$) olup, hafif negative Eu anomalisi ($\text{Eu}/\text{Eu}^* = 0.61\text{--}0.80$) gösterirler. $\varepsilon_{\text{Nd(i)}}$ değerleri -3.0 ve -4.1 arasında değişirken, $^{87}\text{Sr}/^{86}\text{Sr}_{\text{(i)}}$ değerleri 0.7062 ve 0.707 arasında değişmektedir. Mafik magmatik anklavlар monzogranitlere kıyasla daha yüksek Mg# ($27\text{--}29$), daha düşük silis ($56\text{--}58$) ve alüminyum doygunluk indeksi ($0.9\text{--}1.0$) değerleri içerirler. Sarıosman plutonu'nun gelişiminde plajiyoklas, hornblend ve Fe-Ti oksit fraksiyonlaşması önemli bir rol oynamıştır. Magmanın kristalleşme sıcaklığı $700\text{--}800$ °C arasında olup, Al-hornblend jeobarometresine göre intrüzyon nisbeten sığ bir derinlige (~2 to 7 km) yerleşmiştir. Jeokimyasal ve izotopik veriler, Sarıosman plutonu'nun kaynağının dehydratizasyona uğramış mafik alt kabuk kayaçları olabileceğini göstermektedir.

Anahtar Sözcükler: SHRIMP yaşı, Sarıosman plutonu, mineral kimyası, I-tipi, Sr-Nd izotop jeokimyası, doğu Pontidler

Introduction

I-type, calc-alkaline plutonic rocks are common in many different convergent tectonic settings and include subduction-related and collisional magmatic suites. They are characterised by a large compositional diversity arising from different source compositions, variable melting conditions, fractional crystallisation (FC) and crustal contamination, in addition to the complex chemical and physical interactions between mafic and felsic magmas (DePaolo 1981; Zorpi *et al.* 1991; Roberts & Clemens 1993; Thompson & Connolly 1995; Galan *et al.* 1996; Altherr *et al.* 2000; Altherr & Siebel 2002). Because there is a link between the mineralogy, geochemistry and geodynamic setting of granitoids, compositionally well-characterised granitoids of known age may constrain the evolution and development of the continental crust through geological time (Barbarin 1999).

The Alpine-Himalayan orogenic belt embraces various arc, collisional, and post-collisional geological settings; in addition, magmatic rocks were generated in each of these settings. In this belt, Turkey, as a zone of interaction between Eurasia and Gondwanaland plates, lies in an important geodynamic position. The Pontide unit (Ketin 1966) of Turkey includes various intrusive and eruptive rocks that constitute the widespread eastern Pontide terrane: many of these are related to the convergence of these two plates (Figure 1a).

The eastern Pontides represent a well-preserved arc system (Tokel 1977; Eğin *et al.* 1979; Manetti *et al.* 1983; Gedik *et al.* 1992; Çamur *et al.* 1996; Yılmaz & Boztuğ 1996; Boztuğ *et al.* 2003), resulting from the subduction of the Neotethyan oceanic crust beneath the Eurasian plate during the Senonian. Closure of the Neotethyan Ocean caused a collision

between the Pontide arc and the Tauride-Anatolide platform in the Palaeocene-Early Eocene, and this collision continued until the middle Eocene (Yılmaz & Boztuğ 1996; Yılmaz *et al.* 1997; Okay & Şahintürk 1997).

The contemporary geological setting of the eastern Pontides is mainly the result of three main Neotethyan volcanic cycles during the Jurassic, Late Cretaceous and Eocene (Adamia *et al.* 1977; Eğin *et al.* 1979; Kazmin *et al.* 1986; Korkmaz *et al.* 1995; Çamur *et al.* 1996; Arslan *et al.* 1997, 2000). The intrusive rocks were formed in different geodynamic environments and emplaced at various crustal levels (Boztuğ *et al.* 2003, 2006). Crystallisation ages of these intrusives range from Permo-Carbonifeous (Çoğulu 1975) through Cretaceous-Palaeocene (Delaloye *et al.* 1972; Giles 1974; Taner 1977; Gedikoğlu 1978; Moore *et al.* 1980; Jica 1986; Okay & Şahintürk 1997; Yılmaz *et al.* 2000; Köprübaşı *et al.* 2000; Yılmaz-Şahin 2005; Boztuğ *et al.* 2006; Dokuz *et al.* 2006; Boztuğ 2008; İlbeli 2008; Kaygusuz *et al.* 2008; Kaygusuz & Aydıncakır 2009) to Eocene (Boztuğ *et al.* 2003, 2004; Arslan *et al.* 2004; Karslı *et al.* 2004; Topuz *et al.* 2005; Yılmaz-Şahin 2005) periods (Figure 1b). The compositions of the plutons range from low-K tholeiitic through high-K calc-alkaline metaluminous-peraluminous granites to alkaline syenites (Yılmaz & Boztuğ 1996; Boztuğ *et al.* 2003). The emplacements of these plutons also occurred in a wide spectrum of tectonic settings, ranging from arc-collisional through syn-collisional to postcollisional (Yılmaz & Boztuğ 1996; Okay & Şahintürk 1997; Yılmaz *et al.* 1997; Yeğençil *et al.* 2002; Boztuğ *et al.* 2003; Arslan & Aslan 2005). In the Torul region of the Eastern Pontides, arc-related magmatism developed under a compressional regime and is characterised by the predominance of calc-alkaline granitoids.

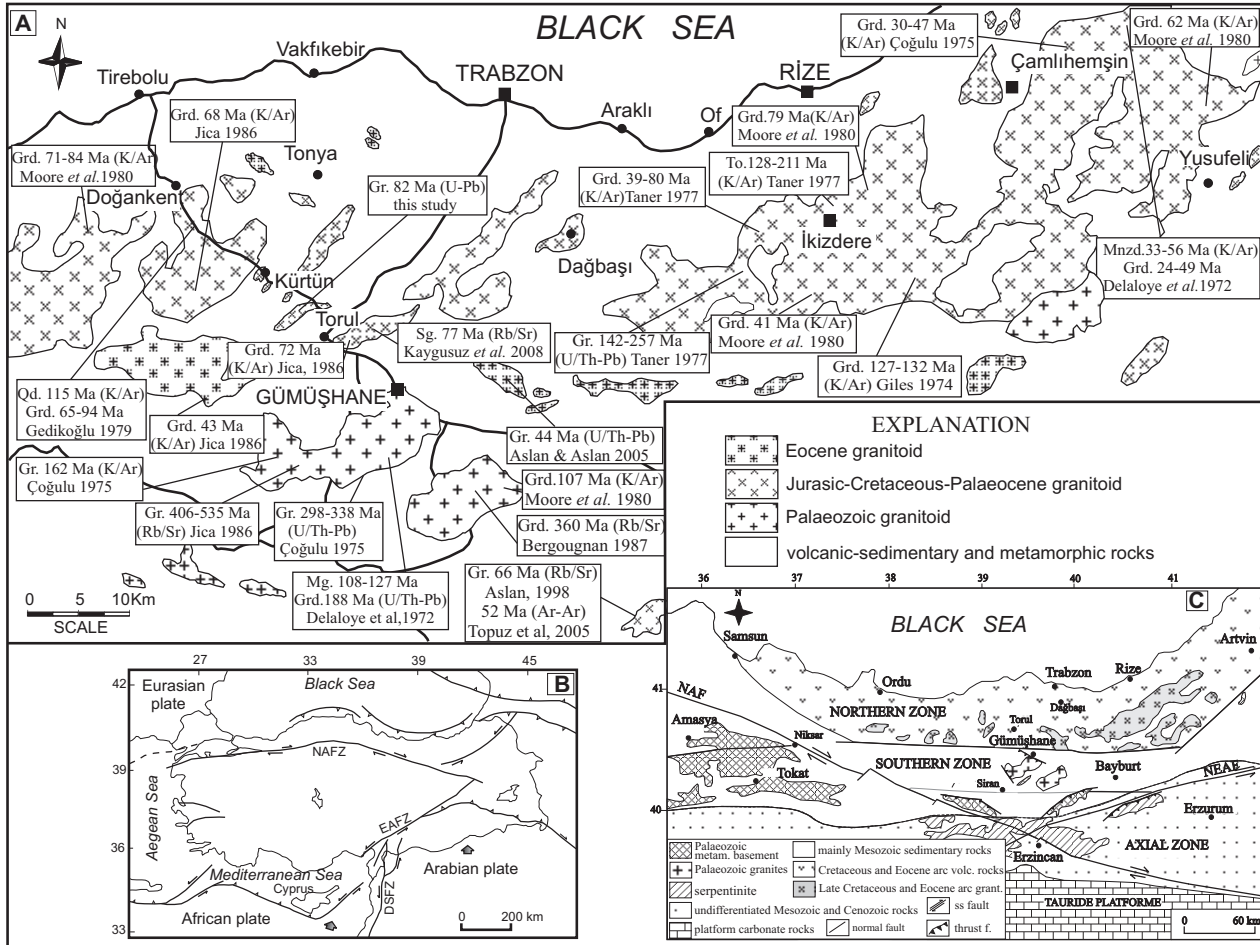


Figure 1. (a) Simplified map showing the main granitoid distribution in the eastern Pontides (modified from Gedik *et al.* 1992 and Güven 1993); (b) Tectonic map of Turkey and surroundings (modified after Şengör *et al.* 2003); and (c) Major structures of the eastern Pontides (modified from Eyüboğlu *et al.* 2007). NAFZ- North-Anatolian fault zone; EAFZ- East-Anatolian fault zone; Grd- granodiorite; Gr- granite; Qd- quartz diorite; Qmz- quartz monzonite; Mnzd- monzodiorite; Sg- syenogranite.

Most of the previous studies in the Eastern Pontides dealt with the general characteristics of the granites within the overall framework of the geological evolution of the region. However, research on the various other aspects of granitoid rocks (namely, age, origin, source and tectonic setting) is rather scarce. The present article focuses mainly on the arc-related granitoids in the eastern Pontides and the interpretation of these granitoids based on their ages, magma sources and geodynamic settings. Before this study, knowledge about the age of the Sariosman intrusions was uncertain, and no geochronological age of this intrusion is currently

available. This article reports new petrographic, geochemical, Sr-Nd isotopic and sensitive high-resolution ion microprobe (SHRIMP) zircon data, in addition to field observations and mineral chemistry from the Sarıosman pluton in the eastern Pontide magmatic arc.

Geological Setting

The eastern Pontides are commonly subdivided into a northern zone and a southern zone, based on the differences between structural and lithological features (Figure 1c) (Akın 1978; Gedikoğlu 1978;

Özsayar *et al.* 1981; Okay & Şahintürk 1997). Late Cretaceous and Middle Eocene volcanic and volcaniclastic rocks dominate the Northern Zone, whereas pre-Late Cretaceous rocks are widely prevalent in the Southern Zone. The basement of the eastern Pontides consists of metamorphic sequences of varying metamorphic grades and is intruded by granitoids of Permian age (Yilmaz 1972; Coğulu 1975; Okay & Şahintürk 1997; Topuz 2002). Volcanic, volcano-sedimentary rocks and local sediments of Liassic–Dogger age (Ağar 1977; Robinson *et al.* 1995) lie unconformably on the basement. These rocks are overlain conformably by Middle and Late Jurassic and Cretaceous carbonates. Some plutonic rocks were emplaced between the Jurassic and Palaeocene periods (Okay & Şahintürk 1997; Yilmaz *et al.* 1997). Subduction-related arc magmatism is recorded by the Senonian submarine volcano-sedimentary units and associated plutonic rocks (Figure 1). Eocene rocks, mainly volcanics and rarely volcanoclastics and sediments, unconformably overlie the Late Cretaceous series (Güven 1993). The Eocene–Neogene volcanic rocks are calc-alkaline to alkaline in composition, although there are lithological and chemical variations between the rocks exposed in the Northern Zone relative to those exposed in the Southern Zone (Arslan *et al.* 1997, 2000; Şen *et al.* 1998). Several granitoids belonging to this magmatic episode intrude the Eocene volcanic and volcaniclastic rocks (Coğulu 1975; Moore *et al.* 1980; Arslan *et al.* 1999). After the end of the Middle Eocene, the region remained largely above sea level, with minor volcanism and terrigenous sedimentation continuing until the present (Okay & Şahintürk 1997).

The Sarıosman pluton is an elliptical body covering an area of approximately 20 km² with its long axis extending NE–SW. The pluton is located within the northern zone of the eastern Pontides about 15 km north of Gümüşhane (Kaygusuz & Şen 1998) (Figure 2). The country rocks around the pluton consist of Late Cretaceous basic and acidic volcanic rocks interbedded with sedimentary strata. Field observations show that the Sarıosman pluton cuts early Cretaceous formations and is itself cut by approximately 5- to 10-m-thick dacitic and 5- to 35-cm-thick aplitic dykes (Kaygusuz 2000).

The Sarıosman pluton can be subdivided into two units, (1) a dominant biotite-hornblende monzogranite unit and (2) a younger small stock of porphyritic hornblende-biotite monzogranite, which intrudes the hornblende-biotite monzogranites and forms a small outcrop at the centre of the elliptically shaped pluton (Figure 2). Pink to pinkish grey biotite-hornblende monzogranites, that constitute ~90% of the mass volume of the pluton, are medium-grained. The pinkish grey porphyritic hornblende-biotite monzogranites are fine- to medium-grained and feldspar phryic. The internal contacts between all these rocks are gradational. In the eastern part of the intrusion, a number of mafic microgranular enclaves (MMEs) with ellipsoidal shapes (up to 10 cm in diameter) occur. Their contacts with the host biotite-hornblende monzogranites vary from sharp to gradational.

Analytical Methods

50 rock samples were collected from the Sarıosman intrusion. The modal mineralogy of 25 samples was determined by point counting with a Swift automatic counter fitted to a polarising microscope. On each thin section, a total of 1300–1500 points were counted and the modes were normalised to 100% (Table 1).

Based on these microscopic studies, 20 of the freshest and most representative rock samples were selected for whole-rock major-element, trace-element and rare earth-element (REE) analyses. Major and trace elements were determined by inductively coupled plasma (ICP)-emission spectrometry and ICP-mass spectrometry at ACME Analytical Laboratories Ltd., Vancouver (Canada), using standard techniques. Major and trace elements were analysed by ICP using 0.2 g of rock powder fused with 1.5 g LiBO₂ and dissolved in 100 ml of 5% HNO₃. Loss on ignition was determined on dried samples heated to a temperature of 1000 °C. REE analyses were carried out by ICP-MS at ACME. Detection limits ranged from 0.01 to 0.1 wt% for the major oxides, 0.1 to 10 ppm for the trace elements, and 0.01 to 0.5 ppm for REEs.

Mineral analyses of the samples were conducted at the University of New Brunswick Electron

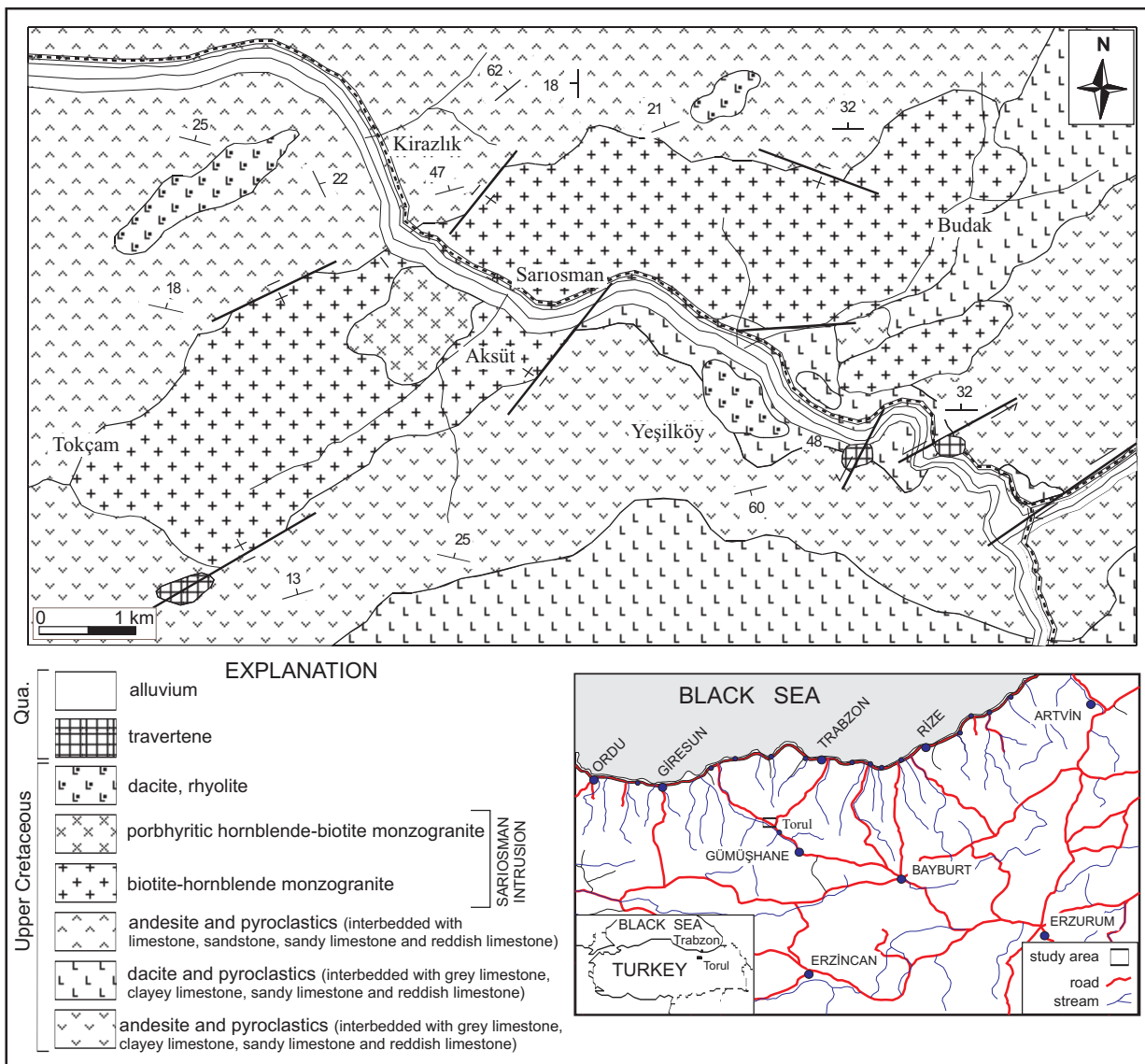


Figure 2. Location and geological map of the study area (modified from Kaygusuz 2000).

Microprobe Laboratory (Canada) with a JEOL JSM-6400 scanning electron microscope, equipped with a Link eXL energy-dispersive analyser and a single-wavelength dispersive channel. X-ray analyses were carried out at an acceleration potential of 15 kV under sample currents of 2.5 nA, using a live time of 100 s for energy-dispersive data acquisition. Data were reduced with the Link ZAF procedure using a combination of mineral (orthoclase-K, albite-Na, hornblende-Al, olivine-Mg, pyroxene-Si, K, Ca and metals such as Fe and Ti) standards. The analytical

results are presented in Tables 2, 3 & 4. Detection limits are generally about 0.1 wt%.

Zircons were set in an epoxy mount, polished to expose the grain centres and vacuum-coated with a 500-nm layer of high-purity gold. U-Pb dating of zircon was carried out at the Beijing SHRIMP Laboratory following the analytical procedures described by Williams (1998). Uranium, Th and Pb abundances were measured based on the standard Sri Lankan zircon SL13, with $U = 238$ ppm and $t = 572$ Ma. Lead ratios were corrected for common Pb using

Table 1. General petrographic features of the various rock types from the Sariosman intrusions.

Rock Unit	Biotite hornblende monzogranite (n=13)	Porphyritic hornblende biotite monzogranite (n=7)	MME (Qtz monzodiorite) (n=5)
Texture	Hypidiomorphic	Hypidiomorphic-porphyritic	Hypidiomorphic-allotriomorphic
Grain Size	Medium	Fine to medium	Fine
Modal Min (%)	Min-max	Min-max	Min-max
Plagioclase	30–40	24–34	60–63
K-Feldspar	25–36	36–41	12–15
Quartz	17–28	22–29	10–13
Hornblende	3–8	1–3	5–8
Biotite	1–3	3–5	1–2
Mineral Chemistry			
Plg (An%)	29–43	21–40	35–46
K-Feld (Or%)	71–90	90–97	–
Bt (Mg#)	0.65–0.66	0.67–0.68	0.70–0.72
Bt - TiO ₂ (wt%)	0.02–0.10	0.04–0.07	0.05–0.18
Hbl (Mg#)	0.65–0.88	0.97–1.0	0.82–0.83
Accessory Phases	titanite, apatite, zircon, epidote, opaques	titanite, apatite, zircon, epidote, opaques	apatite, zircon, epidote, opaques
Secondary Minerals	sericite, carbonate, chlorite, clay minerals	sericite, chlorite, clay minerals	sericite, chlorite, clay minerals

n- sample number, Min- minimum values, max- maximum values, Qtz- quartz, Bt- biotite, Hbl- hornblende, Plg- plagioclase, K-feld- K-feldspar, MME- mafic microgranular enclaves

the measured nonradiogenic ²⁰⁴Pb. The SQUID 1.0 and ISOPLOT softwares of Ludwig (2003) were used for data processing. Regarding the Mesozoic age of the Sariosman pluton, the ²⁰⁶Pb/²³⁸U age is considered the most precise age, because low count rates of ²⁰⁷Pb result in large statistical uncertainties in the ²⁰⁷Pb/²³⁵U and the ²⁰⁷Pb/²⁰⁶Pb ages.

Nd-Sr isotopic analyses were conducted at the Institute of Geology and Geophysics, Chinese Academy of Sciences, Beijing. Samples were dissolved in acid (HF + HClO₄) in sealed Savillex beakers on a hot plate for one week. Separation of Rb, Sr and light REEs was achieved through a cation-exchange column (packed with BioRad AG 50W-X8 resin). Sm and Nd were further purified using a second cation-exchange column that was conditioned and eluted with diluted HCl. Mass

analyses were conducted using a multicollector VG354 mass spectrometer as described by Qiao (1988). ⁸⁷Sr/⁸⁶Sr and ¹⁴³Nd/¹⁴⁴Nd ratios were corrected for mass fractionation relative to ⁸⁶Sr/⁸⁸Sr = 0.1194 and ¹⁴⁶Nd/¹⁴⁴Nd = 0.7219, respectively. Finally, the ⁸⁷Sr/⁸⁶Sr ratios were adjusted to the NBS-987 Sr standard = 0.710250, and the ¹⁴³Nd/¹⁴⁴Nd ratios, to the La Jolla Nd standard = 0.511860. The uncertainty in concentration analyses by isotopic dilution is 2% for Rb, 0.5% for Sr, and 0.2–0.5% for Sm and Nd depending upon concentration levels. Procedural blanks are: Rb= 80 pg, Sr= 300 pg, Sm= 50 pg and Nd= 50–100 pg. Detailed explanation of sample preparation, errors and analytical precision is provided in Zhang *et al.* (2002).

Results

Petrography

The petrographic characteristics of the Sariosman pluton are presented in Table 1. The rocks plot in the monzogranite field and have a calc-alkaline trend (Lameyre & Bowden 1982) in the quartz-alkali feldspar-plagioclase (QAP) modal classification (Streckeisen 1976) diagram (Figure 3).

Rock samples from the pluton are generally holocrystalline, fine- to medium-grained, porphyric, poikilitic, and myrmekitic, rarely micrographic, (Figure 4A–C) in texture. In the centre of the pluton, medium-grained textures predominate, whereas towards the contacts with the volcanic country rocks, the granitoids become finer-grained. Porphyritic textures, with K-feldspar (up to 3.5 mm) and plagioclase (up to 2.5 mm) phenocrysts set in a finer-grained matrix of plagioclase, K-feldspar, quartz, hornblende, biotite and Fe-Ti oxides, are generally displayed by the porphyritic hornblende-biotite monzogranites. Aplites have a granular allotriomorphic texture. The major rock-forming mineral assemblage of the intrusion is K-feldspar, plagioclase, quartz, hornblende, biotite and minor tremolite-actinolite. Titanite, allanite, apatite, zircon, epidote and opaque minerals are accessory phases. Secondary minerals comprise chlorite, calcite, sericite and clay minerals.

Plagioclase forms subhedral to anhedral, normally and reversely zoned prismatic and lath-shaped crystals. Grain sizes range from 0.3 mm for inclusions to 2 mm for larger crystals, some of which may poikilitically contain small plagioclase, hornblende and biotite inclusions. Myrmekitic textures were observed at grain boundaries between plagioclase and orthoclase. Some large plagioclase crystals are altered to sericite and clay minerals. Quartz is anhedral and generally shows undulose extinction. Its grain size decreases in the contact zones between the different rock types. K-feldspar forms anhedral, rarely subhedral, crystals of perthitic orthoclase. Phenocrysts (up to 3.5 mm) were generally observed in the porphyritic hornblende-biotite monzogranites (Figure 4B, C) to poikilitically enclose abundant inclusions of plagioclase, biotite, hornblende and opaque minerals (Figure 4B). Hornblende occurs as euhedral to subhedral tabular,

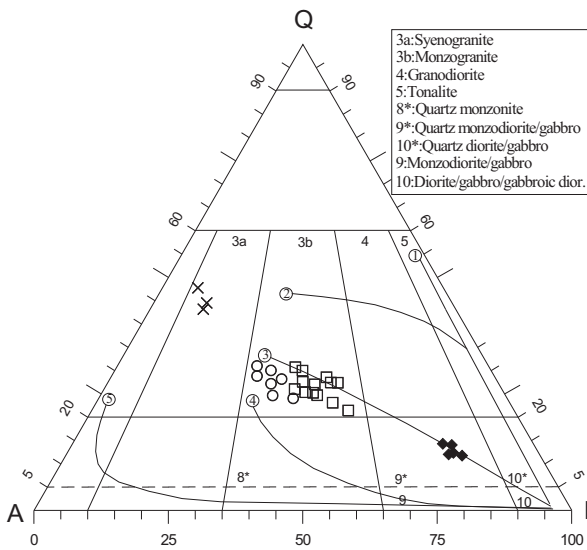


Figure 3. Classification based on modal compositions of the Sariosman intrusions (Streckeisen 1976). Arrows show typical differentiation trends (after Lameyre & Bowden 1982) for various magmatic series: tholeiitic (1), K₂O-poor calc-alkaline (2), intermediate K₂O content calc-alkaline (3), K₂O-rich calc-alkaline (4), alkaline (5).

prismatic and acicular crystals, which are abundant in the biotite-hornblende monzogranite. Towards the intrusion margins, hornblende is increasingly altered to chlorite, calcite and actinolite. Some large hornblende crystals (up to 2.5 mm) may contain small biotite and plagioclase inclusions (Figure 4E). Reddish-brown biotite is euhedral or subhedral and forms prismatic crystals and lamellae. It is abundant in the porphyritic hornblende-biotite monzogranites. In some samples, biotite is altered into chlorite, epidote and opaque minerals along the cleavage planes. Some biotite crystals have poikilitic textures, in which large plagioclase crystals (up to 2.5 mm) may contain small crystals of plagioclase and opaque minerals. Titanite forms euhedral and subhedral crystals in all rock types. Allanite occurs as euhedral, reddish crystals. Needle-like crystals of apatite are mainly found in plagioclase. Zircon was observed as short euhedral and prismatic crystals within all rock types.

MMEs have a quartz monzodioritic composition (Figure 3), and are texturally and mineralogically similar to their host biotite-hornblende

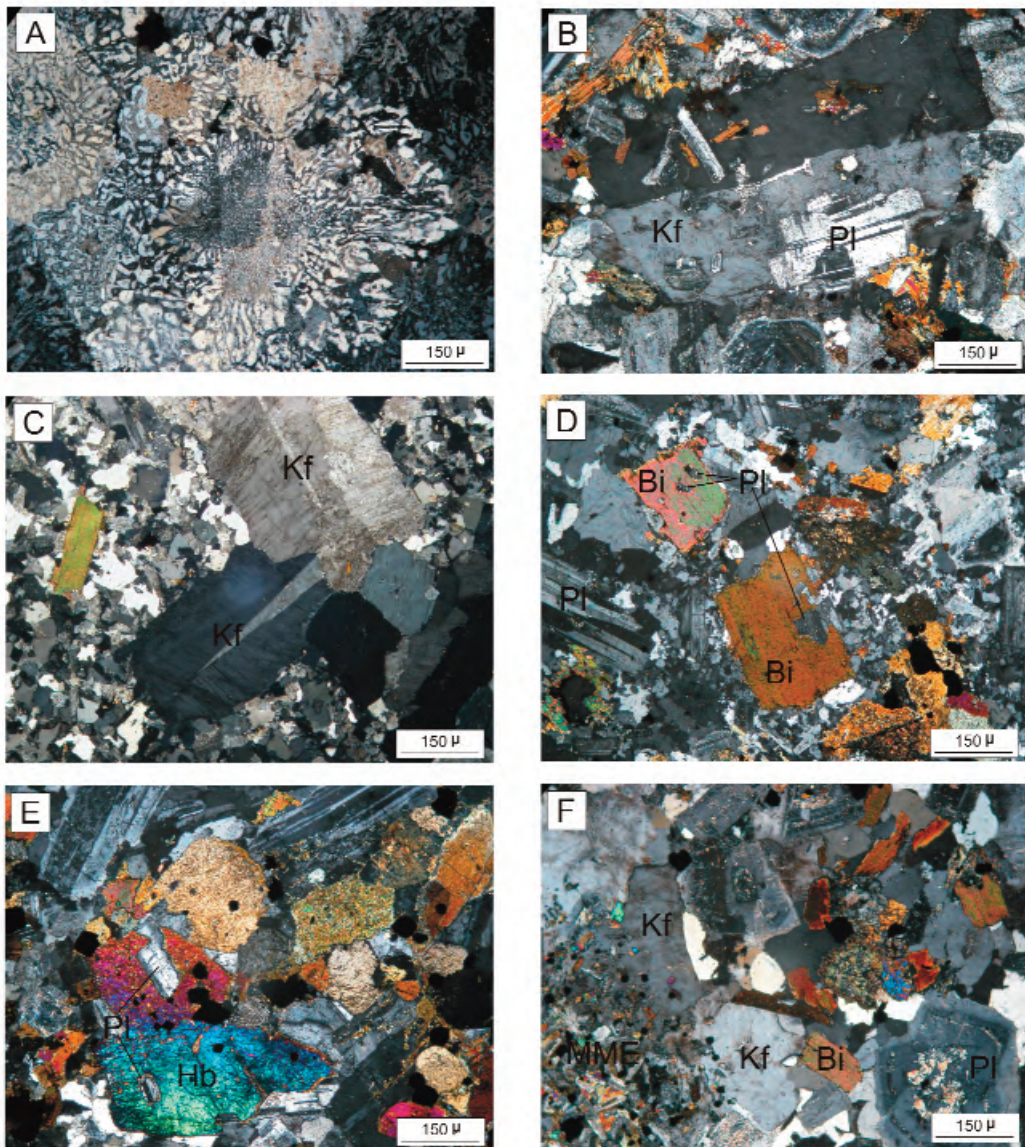


Figure 4. Micrographs showing certain textural features of the Sariosman intrusions and associated rocks: (A) graphic texture; (B) poikilitic texture in K-feldspar, in which some large K-feldspar may contain small plagioclase, hornblende and biotite crystals; (C) K-feldspar megacrysts; (D) plagioclase and opaque mineral inclusions in large biotite crystals; (E) small plagioclase and opaque mineral inclusions in large hornblende crystals; (F) large K-feldspar crystals at the contact region of MMEs and host rocks. Pl- plagioclase, Kf- K-feldspar, Bi- biotite, Hb- hornblende, Q- quartz, Op- opaque minerals.

monzogranites (Table 1). They mineralogically contain plagioclase, K-feldspar, quartz, hornblende and biotite as major constituents, and apatite, zircon and opaque minerals as the accessory phases. The MMEs contain higher proportions of ferromagnesian phases and plagioclase and lower

proportions of quartz and K-feldspar compared to the host rocks. Plagioclase is subhedral and has albite-law twinning. Hornblende is the most abundant mafic mineral in the MMEs, and biotite is abundant at the contact regions between the enclave and host rock.

Dacitic dykes are porphyritic, with phenocrysts of plagioclase, biotite and hornblende (0.3–2.0 mm) in a fine-grained matrix of quartz, plagioclase, hornblende, biotite, orthoclase, Fe-Ti oxide and apatite. Biotite phenocrysts often contain relatively large inclusions of plagioclase and opaque minerals. Hornblende forms needles and is largely altered to chlorite and calcite. Aplitic dykes consist of quartz, orthoclase, plagioclase and minor biotite, apatite, zircon and titanite. Some of these dykes are composite, with quartz-rich inner zones.

Mineral Chemistry

Plagioclase- Compositions of plagioclase crystals from biotite-hornblende monzogranites, porphyritic hornblende-biotite monzogranites and MMEs are provided in Table 2. A narrow range of oligoclase to andesine (An_{21} to An_{43}) can be found. The composition is andesine (An_{29} to An_{43}) in biotite-hornblende monzogranites and oligoclase-andesine (An_{21} to An_{40}) in hornblende-biotite monzogranites (Figure 5; Table 2). The MMEs have more calcic plagioclase (An_{36} to An_{46}) than the host biotite-hornblende monzogranites. The anorthite component decreases from the margin to the centre of the intrusion. Normally zoned plagioclases have $\sim An_{43}$ in the cores and $\sim An_{30}$ at the rims (Table 2).

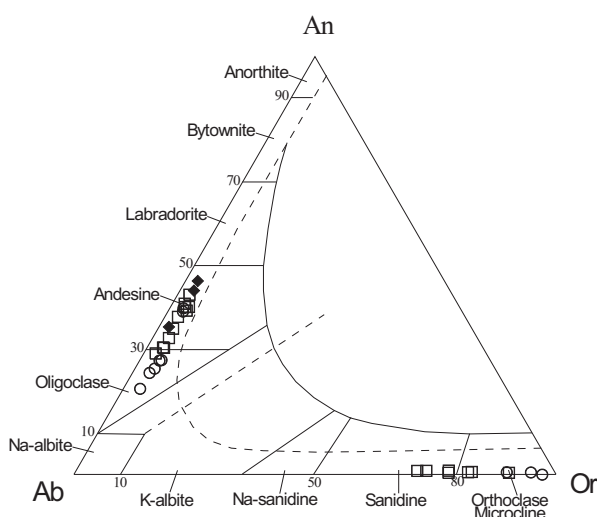


Figure 5. Chemical compositions of plagioclase and K-feldspar from the Sariosman intrusions.

K-feldspar- Compositions of K-feldspar from all rock types are presented in Table 3. Its composition is characterised by a variation in orthoclase content, ranging from Or_{71} to Or_{97} (Figure 5; Table 3). The composition ranges from Or_{71} to Or_{90} in biotite-hornblende monzogranites and Or_{90} to Or_{97} in porphyritic hornblende-biotite monzogranites (Figure 5, Table 3).

Hornblende- Hornblende is the most common ferromagnesian mineral in all rock types. The results of representative analysis are shown in Table 4. Its composition varies from Mg-hornblende through actinolitic hornblende to tremolitic hornblende of the calcic group (Leake *et al.* 1997) (Figure 6). In the biotite-hornblende monzogranites, Mg-hornblende and actinolitic hornblende occur, whereas Mg-hornblende and tremolitic hornblende are found mainly in the porphyritic hornblende-biotite monzogranites. MME amphiboles can be classified as Mg-hornblende (Figure 6). The Mg-number of the amphiboles ((Mg# = atomic ratios of Mg/(Mg + Fe), where Fe is total iron) varies between 0.65 and 1.0 (Table 4). The MMEs have intermediate Mg-numbers (0.82–0.83) compared to the other rock types. An increasing Mg/Mg+Fe²⁺ ratio with increasing Si per formula unit of hornblendes can be observed in all rock types.

Biotite- The results of representative biotite analyses are provided in Table 4. The biotite of all rock types and MMEs is Fe-rich ($Fe^{2+}/(Fe^{2+}+Mg)$ = 0.28–0.35; Figure 7a; Table 4); although some biotites are transitional to Mg-biotite (Figure 7a). They are rich in TiO_2 and MgO and plot within the calc-alkaline field in the $MgO-FeO^T-Al_2O_3$ diagram (Nachit *et al.* 1985) (Figure 7b). The Mg-number varies between 0.65 and 0.68 in all rock types and between 0.70–0.72 in the MMEs (Table 4).

Thermobarometry

The Sariosman intrusions contain the critical mineral assemblage of [K-feldspar + quartz + plagioclase + hornblende + biotite + apatite + zircon + titanite + Fe-Ti oxide] for application in the Al-in-hornblende barometer (Hammastrom & Zen 1986;

Table 2. Microprobe analysis of plagioclase from the Sariosman intrusions.

Rock types	Plagioclase												MME								
	Biotite hornblende monzogranite												Porphyritic hornblende biotite monzogranite								
	A4-1	A20-1	A20-2	A20-3	A20-4	A20-5	A30-1	A30-2	A30-3	A21-1	A21-2	A30-1	A30-2	A30-3	A30-4	A21-1	A30-1	A21-3	A4-1	A4-2	A4-3
SiO ₂	61.07	57.28	58.40	59.86	60.33	60.34	57.82	57.96	57.83	60.19	58.51	60.98	61.04	62.85	62.33	57.88	58.13	61.88	56.44	59.74	56.49
TiO ₂	0.04	0.00	0.00	0.00	0.04	0.03	0.01	0.08	0.00	0.08	0.02	0.04	0.00	0.00	0.03	0.07	0.08	0.00	0.00	0.07	0.00
Al ₂ O ₃	23.68	26.45	25.50	24.52	24.09	24.21	26.22	25.98	25.85	25.58	25.70	23.98	23.99	22.85	23.69	25.33	25.43	23.33	26.30	24.66	26.77
FeO ^T	0.17	0.25	0.23	0.18	0.22	0.26	0.29	0.27	0.28	0.25	0.31	0.19	0.17	0.21	0.20	0.27	0.31	0.21	0.30	0.65	0.24
MgO	0.01	0.01	0.01	0.02	0.01	0.00	0.00	0.04	0.02	0.03	0.00	0.00	0.00	0.00	0.00	0.03	0.01	0.00	0.02	0.02	0.02
CaO	6.05	9.22	8.20	7.12	6.63	6.56	8.73	8.64	8.60	7.44	8.11	5.95	5.86	4.55	5.48	8.24	8.20	5.30	9.51	7.12	9.84
Na ₂ O	7.92	6.46	7.16	7.72	8.01	7.92	6.69	6.78	6.65	7.30	6.52	8.29	8.08	9.34	8.45	6.57	6.73	8.70	6.34	6.98	6.01
K ₂ O	0.44	0.44	0.50	0.62	0.65	0.60	0.46	0.55	0.69	0.56	0.66	0.76	0.81	0.66	0.75	0.50	0.56	0.65	0.53	0.35	0.46
Total	99.4	100.1	100.0	100.0	99.9	100.2	100.3	99.9	101.4	99.8	100.2	99.9	100.4	100.5	100.9	98.7	99.4	100.1	99.4	99.6	99.8
Si	2.73	2.57	2.62	2.68	2.70	2.70	2.59	2.60	2.60	2.65	2.63	2.72	2.72	2.78	2.75	2.63	2.62	2.75	2.56	2.68	2.55
Ti	0.00	0.00	0.00	0.00	0.00	0.00	0.00	0.00	0.00	0.00	0.00	0.00	0.00	0.00	0.00	0.00	0.00	0.00	0.00	0.00	0.00
Al	1.25	1.40	1.35	1.29	1.27	1.28	1.39	1.37	1.37	1.33	1.36	1.26	1.26	1.19	1.23	1.36	1.35	1.22	1.41	1.30	1.42
Fe ²⁺	0.01	0.01	0.01	0.01	0.01	0.01	0.01	0.01	0.01	0.01	0.01	0.01	0.01	0.01	0.01	0.01	0.01	0.01	0.01	0.02	0.01
Mg	0.00	0.00	0.00	0.00	0.00	0.00	0.00	0.00	0.00	0.00	0.00	0.00	0.00	0.00	0.00	0.00	0.00	0.00	0.00	0.00	0.00
Ca	0.29	0.44	0.39	0.34	0.32	0.31	0.42	0.42	0.41	0.35	0.39	0.28	0.28	0.22	0.26	0.40	0.40	0.25	0.46	0.34	0.48
Na	0.69	0.56	0.62	0.67	0.69	0.69	0.58	0.59	0.58	0.62	0.57	0.72	0.70	0.80	0.72	0.58	0.59	0.75	0.56	0.61	0.53
K	0.03	0.03	0.03	0.04	0.04	0.03	0.03	0.04	0.03	0.04	0.03	0.04	0.04	0.05	0.04	0.03	0.03	0.04	0.03	0.02	0.03
An	28.94	43.01	37.71	32.63	30.29	30.36	40.85	40.06	40.08	34.87	39.19	27.24	27.34	20.48	25.31	39.76	38.97	24.28	43.98	35.28	46.28
Ab	68.56	54.52	59.55	63.97	66.16	66.34	56.59	56.89	56.09	61.99	57.01	68.61	68.15	76.01	70.59	57.39	57.89	72.16	53.10	62.64	51.16
Or	2.49	2.47	2.74	3.40	3.55	3.30	2.56	3.05	3.83	3.14	3.80	4.15	4.52	3.51	4.10	2.85	3.14	3.56	2.92	2.07	2.56

Structural formula on the basis of 8 oxygen atoms

FeO^T is total iron as FeO, MME— mafic microgranular enclaves, Qtz— quartz

Table 3. Microprobe analysis of K-feldspar from the Sarıosman intrusions.

Rock types	K-feldspar							Porphyritic hbl-bi monzogranite		
	Biotite hornblende monzogranite									
Samples	A20-1	A30-1	A30-2	A4-1	A4-2	A4-3	A21-1	A30-1	A21-1	A21-2
SiO ₂	64.58	65.56	65.99	65.75	64.88	64.08	64.62	64.66	64.85	63.84
TiO ₂	0.03	0.04	0.00	0.05	0.08	0.06	0.02	0.00	0.01	0.04
Al ₂ O ₃	17.89	18.19	18.45	18.46	18.12	18.20	18.24	17.99	17.74	17.73
FeO ^T	0.04	0.04	0.11	0.05	0.07	0.07	0.10	0.04	0.11	0.03
MgO	0.01	0.01	0.00	0.02	0.01	0.00	0.01	0.00	0.02	0.01
CaO	0.08	0.12	0.18	0.19	0.11	0.08	0.18	0.10	0.11	0.01
Na ₂ O	1.12	2.01	3.37	2.51	2.01	2.46	3.05	0.57	1.16	0.33
K ₂ O	16.08	14.64	12.79	13.52	13.86	13.12	12.71	16.40	15.90	16.91
Total	99.8	100.6	100.9	100.4	99.1	98.1	98.9	99.7	99.9	98.8
Si	3.00	3.00	2.99	3.00	3.00	2.99	2.99	3.00	3.01	3.00
Ti	0.00	0.00	0.00	0.00	0.00	0.00	0.00	0.00	0.00	0.00
Al	0.98	0.98	0.99	0.99	0.99	1.00	1.00	0.98	0.97	0.98
Fe ²⁺	0.00	0.00	0.00	0.00	0.00	0.00	0.00	0.00	0.00	0.00
Mg	0.00	0.00	0.00	0.00	0.00	0.00	0.00	0.00	0.00	0.00
Ca	0.00	0.01	0.01	0.01	0.01	0.00	0.01	0.00	0.01	0.00
Na	0.10	0.18	0.30	0.22	0.18	0.22	0.27	0.05	0.10	0.03
K	0.95	0.85	0.74	0.79	0.82	0.78	0.75	0.97	0.94	1.01
An	0.38	0.59	0.84	0.90	0.53	0.39	0.86	0.47	0.50	0.06
Ab	9.57	17.17	28.35	21.78	17.98	22.10	26.46	4.95	9.95	2.87
Or	90.05	82.24	70.81	77.31	81.49	77.51	72.68	94.58	89.54	97.18

Structural formula on the basis of 8 oxygen atoms

FeO^T is total iron as FeO, MME– mafic microgranular enclaves, hbl– hornblende, bi– biotite

Anderson & Smith 1995; Hollister *et al.* 1987) and hornblende-plagioclase thermometer (Blundy & Holland 1990). Great care has been taken to measure the rims of the crystals in equilibrium to estimate the approximate P-T values. Although the cores and rims of the amphiboles show no significant difference in Al content, the rim composition of the amphibole in contact with interstitial quartz and/or

orthoclase has been used for the calculation representing the late stage (near-solidus) crystallisation of the magma. The results are shown in Table 5. Accordingly, the pressures obtained from the rocks of the pluton range from 0.2 to 2.3 kbar, and the temperatures from 717 to 814 °C. These values correspond to shallow-level emplacement depths between ~ 2 and 7 km.

Table 4. Microprobe analyses of hornblende and biotite from the Sarosman intrusions.

Rock types	Hornblende										Biotite									
	Biotite-hornblende monzogranite					Porphyritic hbl-bio mg					MME		MME		Qtz mnzdi					
	A20-1	A20-2	A30-1	A30-2	A4-1	A4-2	A4-3	A30-1	A21-1	A21-2	A4-1	A4-2	Samples	Rock types	Bio-hbl mg	Porphyritic hbl-bi mg	Qtz mnzdi			
SiO ₂	51.05	50.35	50.10	51.09	50.14	49.01	48.27	47.11	47.35	47.82	45.00	44.66	SiO ₂	39.55	38.07	38.04	39.74	37.97	39.87	
TiO ₂	1.15	1.60	1.36	0.63	1.16	0.44	1.19	0.15	0.14	0.11	1.04	1.41	TiO ₂	0.07	0.10	0.02	0.07	0.04	0.18	0.05
Al ₂ O ₃	5.61	4.78	4.93	5.92	5.55	5.87	6.57	5.32	4.88	5.62	6.67	9.65	Al ₂ O ₃	19.63	19.60	19.19	19.91	19.01	19.85	18.57
FeO ^T	13.17	14.51	13.98	14.19	12.16	12.28	12.74	11.04	11.73	11.07	12.67	14.00	FeO ^T	16.28	17.29	17.10	16.24	15.32	15.28	14.06
MgO	14.00	15.06	14.04	15.07	15.57	15.62	14.92	15.00	14.01	15.02	14.98	13.38	MgO	18.11	18.04	17.94	18.13	18.11	19.58	20.19
CaO	9.92	9.39	9.43	9.58	11.76	11.75	11.78	13.73	14.23	14.47	12.00	11.82	CaO	0.08	0.15	0.10	0.08	0.13	0.12	0.14
Na ₂ O	0.05	0.02	0.00	0.01	1.19	1.17	1.32	0.02	0.02	0.00	1.19	1.58	Na ₂ O	0.02	0.00	0.01	0.02	0.02	0.04	0.04
K ₂ O	0.00	0.03	0.03	0.01	0.50	0.56	0.67	0.01	0.02	0.03	0.79	1.01	K ₂ O	0.02	0.03	0.02	0.02	0.03	0.03	0.18
Total	94.94	95.74	93.87	96.50	98.03	96.70	97.46	92.39	92.36	94.13	94.35	97.51	Total	93.74	93.27	92.92	92.49	92.39	93.04	93.11
Si	7.34	7.13	7.27	7.15	7.17	7.09	6.99	7.20	7.28	7.19	6.76	6.54	Si	5.63	5.49	5.57	5.50	5.71	5.44	5.67
Ti	0.12	0.17	0.15	0.07	0.12	0.05	0.13	0.02	0.02	0.01	0.12	0.15	Ti	0.01	0.01	0.00	0.01	0.00	0.02	0.01
Al ⁴	0.66	0.80	0.73	0.85	0.83	0.91	1.01	0.80	0.72	0.81	1.18	1.46	Al	3.29	3.33	3.27	3.39	3.22	3.35	3.11
Al ⁶	0.29	0.00	0.12	0.13	0.10	0.09	0.11	0.15	0.17	0.19	0.00	0.21	Fe ²⁺	1.94	2.09	2.07	1.96	1.84	1.83	1.67
Fe ²⁺	1.05	1.72	1.38	1.66	0.46	0.64	0.50	0.11	0.00	0.00	0.71	0.59	Mg	3.84	3.88	3.86	3.91	3.88	4.18	4.28
Fe ³⁺	1.05	1.72	1.38	1.66	0.46	0.64	0.50	0.11	0.00	0.00	0.71	0.59	Ca	0.01	0.02	0.02	0.01	0.02	0.02	0.02
Mg	3.00	3.18	3.04	3.14	3.32	3.37	3.22	3.42	3.21	3.37	3.35	2.92	Na	0.01	0.00	0.00	0.01	0.01	0.01	0.01
Ca	1.53	1.43	1.47	1.44	1.80	1.82	1.83	2.25	2.35	2.33	1.93	1.86	K	0.00	0.01	0.00	0.00	0.00	0.01	0.03
Na	0.01	0.01	0.00	0.00	0.33	0.33	0.37	0.01	0.00	0.00	0.35	0.45	Mg [#]	0.66	0.65	0.65	0.67	0.68	0.70	0.72
K	0.00	0.01	0.00	0.00	0.09	0.10	0.12	0.00	0.00	0.01	0.15	0.19	Fe ²⁺ /Fe ³⁺ /Mg	0.34	0.35	0.35	0.33	0.32	0.30	0.28
Mg [#]	0.74	0.65	0.69	0.65	0.88	0.84	0.87	0.97	1.00	1.00	0.82	0.83								

Structural formula on the basis of 23 oxygen

FeO^T is total iron as FeO, MME- mafic microgranular enclaves, hbl- hornblende, bi- biotite, Qtz- quartz, mnzdi- monzodiorite, mg- monzogranite

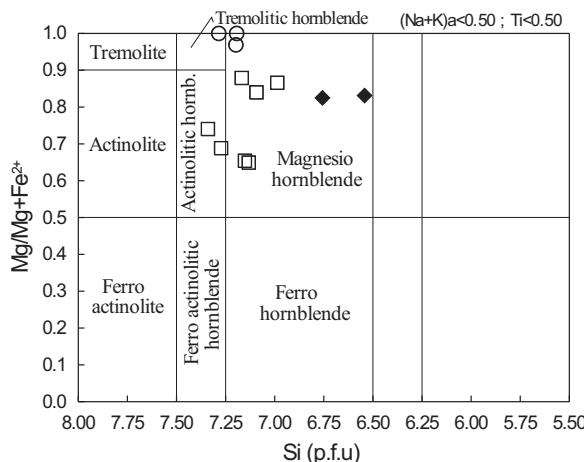


Figure 6. Composition and classification (Leake *et al.* 1997) of hornblendes from the Sariosman intrusions.

U-Pb SHRIMP Zircon Ages

Single zircons from a hornblende-biotite monzogranite sample of the Sariosman pluton were analysed by the SHRIMP dating technique; the results are summarised in Table 6 and in the Concordia diagram of Figure 8. Zircons are colourless to light yellow, long prismatic and perfectly euhedral. Most analyses yield concordant age data. Twelve spot analyses have yielded $^{206}\text{Pb}/^{238}\text{U}$ ages ranging from 78 to 87 Ma, with a weighted mean value of 82.7 ± 1.5 Ma (mean square weighted deviate = 1.4) (Table 6; Figure 8). In determining the Mesozoic age of the Sariosman pluton, the $^{206}\text{Pb}/^{238}\text{U}$ age is considered the most precise age, because low count rates of ^{207}Pb result in large statistical uncertainties in the $^{207}\text{Pb}/^{235}\text{U}$ and the $^{207}\text{Pb}/^{206}\text{Pb}$ ages.

Whole-rock Geochemistry

Major and trace element chemical analyses of representative samples from the Sariosman pluton, including that of the REEs, are detailed in Table 7. In the classification diagram of Debon & Le Fort (1982), the samples plot in the monzogranite field and their MMEs plot in the quartz monzodiorite and quartz monzonite fields (Figure 9). Applying the granite classification scheme of Frost *et al.* (2001), all samples can be classified as magnesian in the $\text{FeO}^T/(\text{FeO}^T + \text{MgO}) - \text{SiO}_2$ diagram (Figure 10a)

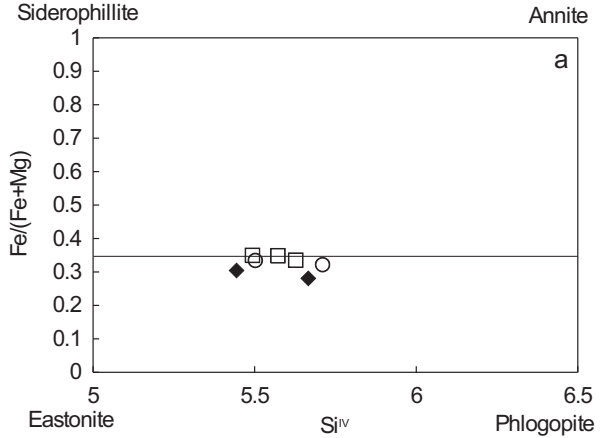


Figure 7. (a) $(Fe/Fe+Mg)$ vs. Si^{IV} diagram and (b) $\text{FeO}-\text{Al}_2\text{O}_3-\text{MgO}$ ternary diagram (Abdel-Rahman 1994) for biotites from the Sariosman intrusions.

and as calc-alkaline in the modified alkali index vs SiO_2 diagram (Figure 10b). The MMEs plot in the alkali-calcic field of this diagram (Figure 10b). According to Frost *et al.* (2001), Cordilleran-type granitoids tend to be lower in $\text{Na}_2\text{O}+\text{K}_2\text{O}-\text{CaO}$, similar to the Sariosman samples, whereas the Caledonian post-collisional plutons are included largely in the high $\text{Na}_2\text{O}+\text{K}_2\text{O}-\text{CaO}$ field (Figure 10b). On an Rb-Sr-Ba ternary diagram (Tarney & Jones 1994), the samples plot in the field of high Ba-Sr granitoids (Figure 11); they specify calc-alkaline trends on a Na-Ca-K (Figure 12a) and Al-Fe-Mg (AFM) ternary diagrams (Figure 12b).

Table 5. Pressure (kbar)- and temperature (°C)-range estimates from the Sarıosman intrusions.

Rock type	Al (pfu)	Pl (Ab)	P (kbar) ^a	P (kbar) ^b	P (kbar) ^c	T (°C) ^d
Bi-hb-mg						
A20	0.95	54.52	0.86	0.60	1.52	717
A30	0.98	56.09	0.99	0.75	1.64	771
A4	0.93	61.99	0.78	0.51	1.44	776
A4	1.00	57.01	1.12	0.89	1.76	786
A4	1.12	68.56	1.72	1.56	2.33	814
Hb-bi-mg						
A30	0.96	68.61	0.90	0.64	1.55	772
A21	0.88	57.30	0.53	0.23	1.20	742
A21	1.00	72.16	1.09	0.86	1.73	772
MME						
A4	1.18	53.10	2.02	1.90	2.61	851
A4	1.67	51.16	4.46	4.64	4.92	864

Al (pfu)– aluminium per formula, Pl (Ab)– albite content in plagioclase, MME– mafic microgranular enclaves, Bi– biotite, Hb– hornblende, mg– monzogranite

The biotite-hornblende monzogranites and porphyritic hornblende-biotite monzogranites span a narrow compositional range, with SiO₂ between 66 and 70 wt%, whereas the MMEs have SiO₂ between 56 and 58 wt% (Table 7, Figure 13). All the rock types are metaluminous to slightly peraluminous, with aluminium saturation index (ASI) [molar Al₂O₃/(CaO + Na₂O + K₂O)] values ranging from 0.88 to 1.06, and are of the I-type character (Figure 13a). The MMEs have ASI values of 0.86–1.06, similar to those of their host rocks. All samples are subalkaline and belong to the high-K calc-alkaline series (Figure 13b). Harker plots of selected major and trace elements (Figure 13) show systematic variations in element concentration. The rocks define a variation trend without a compositional gap, whereas such a gap exists between the MMEs and the intrusive rock types. CaO, MgO, Al₂O₃, Fe₂O₃, TiO₂, P₂O₅, Ba and Sr contents decrease with increasing SiO₂ content, whereas K₂O, Rb, Pb, Th and Nb increase; Na₂O and Zr are nearly constant (Figure 6b-r). The MMEs have the lowest K₂O, Ba and Th concentrations (Figure 13b, k & o).

Primitive mantle-normalised (Sun & McDonough 1989) element-concentration diagrams are shown in Figure 14a–c. All rocks show enrichment of large-ion lithophile elements (LILE) and depletion of high-field strength elements (HFSE). The depletion in HFSE is best expressed by

negative Nb and Ta anomalies. In addition, negative P and Ti anomalies are found in all rock types (Figure 14a–c). The biotite-hornblende monzogranites and porphyritic hornblende-biotite monzogranites have positive Pb anomalies.

Chondrite-normalised (Taylor & McLennan 1985) REE patterns of all rock types have concave upward profiles ($\text{La}_{\text{cn}}/\text{Lu}_{\text{cn}} = 10.1\text{--}17.4$) and are characterised by negative Eu anomalies ($\text{Eu}/\text{Eu}^* = 0.61\text{--}0.80$) (Figure 15a–c, Table 8). The MMEs display a larger range of Eu anomalies ($\text{Eu}/\text{Eu}^* = 0.58\text{--}0.88$), extending to values lower than those in the other rock types, indicating plagioclase fractionation.

Isotope Geochemistry

Rb-Sr and Sm-Nd isotopic data are listed in Table 9 and plotted in Figure 16a–c. Initial Nd-Sr isotopic compositions were calculated using an age of 82 Ma, based on the results of zircon U-Pb dating. The pluton samples have relatively homogeneous isotopic compositions. Biotite-hornblende monzogranites show a small range of Sr-Nd values (initial $^{87}\text{Sr}/^{86}\text{Sr} = 0.7062$ to 0.7064 ; $\epsilon_{\text{Nd(i)}} = -3.0$ to -3.2). The porphyritic hornblende-biotite monzogranites are displaced towards slightly higher initial $^{87}\text{Sr}/^{86}\text{Sr}$ ratios (0.7063 and 0.7070) and lower $\epsilon_{\text{Nd(i)}}$ values (-3.2 to -4.1) compared to the other samples. The Nd

Table 6. U-Pb SHRIMP analytical data of zircon from the Sariosman intrusions.

Spot	$^{206}\text{Pb}_c$ (%)	U (ppm)	Th (ppm)	$^{232}\text{Th}/^{238}\text{U}$	$^{206}\text{Pb}^*$ (ppm)	$^{206}\text{Pb}/^{238}\text{U}$ age (1)	$\pm 1\sigma$	$^{206}\text{Pb}/^{238}\text{U}$ age (2)	$\pm 1\sigma$	$^{206}\text{Pb}/^{238}\text{U}$ age (3)	$\pm 1\sigma$	$^{207}\text{Pb}^*/^{235}\text{U}$ age (1)	$\pm 1\sigma$	$^{207}\text{Pb}^*/^{235}\text{U}$ age (2)	$\pm 1\sigma$	$^{207}\text{Pb}^*/^{235}\text{U}$ age (3)	$\pm \%$	$^{207}\text{Pb}^*/^{238}\text{U}$ (3)	$\pm \%$
Monzogranite																			
A30-1.1	2.56	516	347	0.69	5.72	80.5	± 3.6	80.1	± 2.7	85.3	± 4.1	39.5	6.2	0.089	12	0.1789	4.9	0.01332	4.5
A30-1.2	4.15	531	351	0.68	6.02	81.1	± 2.8	79.9	± 3.4	85.5	± 3.4	43.1	8.8	0.103	12	0.1842	4.1	0.01335	3.4
A30-1.3	6.39	403	237	0.61	4.87	84.2	± 2.6	83.5	± 2.4	88.7	± 2.9	40	13	0.098	19	0.1794	4.1	0.01385	2.9
A30-1.4	3.95	695	528	0.79	8.11	83.7	± 2.4	83.3	± 2.3	87.5	± 2.8	55.5	6.3	0.092	13	0.1619	3.5	0.01367	2.8
A30-5.1	4.05	360	233	0.67	3.96	78.8	± 2.4	79.5	± 2.3	82.8	± 2.9	43	11	0.068	24	0.1416	4.6	0.01293	2.9
A30-6.1	3.37	423	448	1.09	4.81	81.9	± 3.2	80.8	± 3.1	85.6	± 4.2	63.4	8.1	0.102	13	0.1706	4.6	0.01337	3.8
A30-7.1	4.07	381	231	0.63	4.46	83.7	± 2.6	83.8	± 2.4	87.8	± 2.9	45	± 11	0.083	20	0.1584	4.1	0.01371	2.9
A30-8.1	1.60	509	320	0.65	5.76	83.0	± 2.4	82.5	± 2.3	83.6	± 2.7	77.5	5.6	0.0946	8.2	0.1054	4.3	0.01306	2.9
A30-9.1	2.60	605	398	0.68	6.68	80.2	± 2.8	80.1	± 2.8	82.2	± 3.3	62.9	6.3	0.0841	11	0.1207	4.3	0.01284	3.5
A30-10.1	2.16	618	415	0.69	6.97	82.3	± 2.4	81.7	± 2.3	84.6	± 2.8	62.8	6.8	0.0939	11	0.1361	4.9	0.01321	2.8
A30-11.1	1.88	719	577	0.83	8.59	87.4	± 2.5	87.2	± 2.4	90.0	± 2.9	68.8	5.0	0.0930	9.4	0.1424	3.6	0.01407	2.8
A30-12.1	2.70	490	298	0.63	5.70	84.5	± 3.3	84.3	± 3.3	88.0	± 3.7	50.7	7.4	0.089	13	0.1553	4.8	0.01375	3.9

Errors are 1-sigma; Pb and Pb^* indicate the common and radiogenic portions, respectively.(1) Common Pb corrected using measured ^{206}Pb .(2) Common Pb corrected by assuming $^{206}\text{Pb}/^{238}\text{U}_{-}^{207}\text{Pb}/^{235}\text{U}$ age-concordance(3) Common Pb corrected by assuming $^{206}\text{Pb}/^{238}\text{U}_{-}^{208}\text{Pb}/^{232}\text{Th}$ age-concordanceNote: $^{206}\text{Pb}/^{238}\text{U}$ age (1) values used in the text as the weighted mean

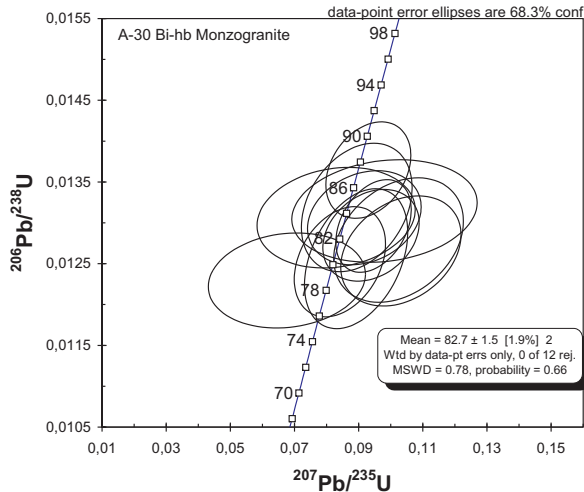


Figure 8. Concordia diagram showing SHRIMP analyses of zircon from a monzogranite (sample A-30) of the Sariosman pluton.

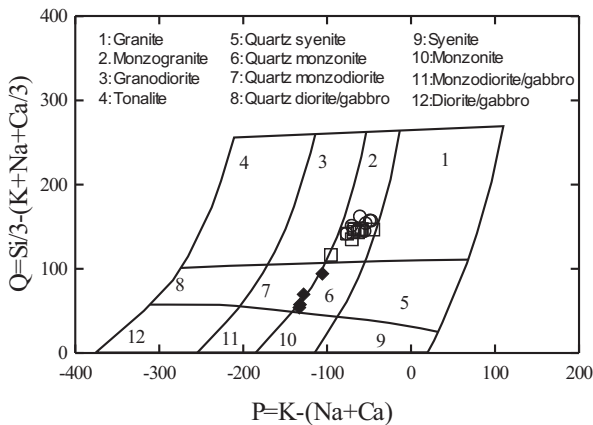


Figure 9. Chemical nomenclature diagram (Debon & Le Fort 1982) for samples from the Sariosman pluton. See Figure 3 for explanation.

model ages (T_{DM}) of all samples are in the range of 0.92–0.99 Ga.

All samples plot on the extension of the mantle array (Figure 16a), pointing towards the field of the lower continental crust, but far away from the field for the upper continental crust (UCC). Sample A40 (from porphyritic hornblende-biotite monzogranite), which plots to the right of the mantle array, may have been slightly contaminated by UCC during magma ascent.

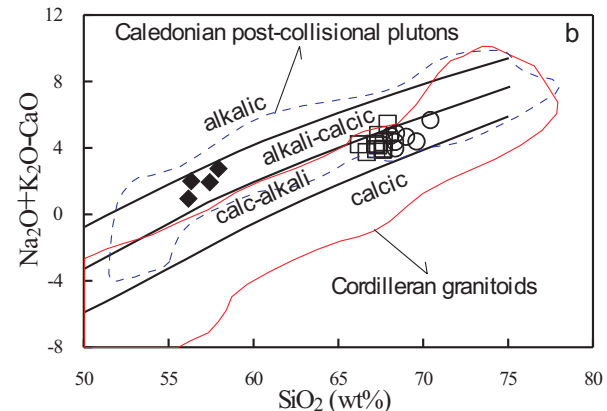
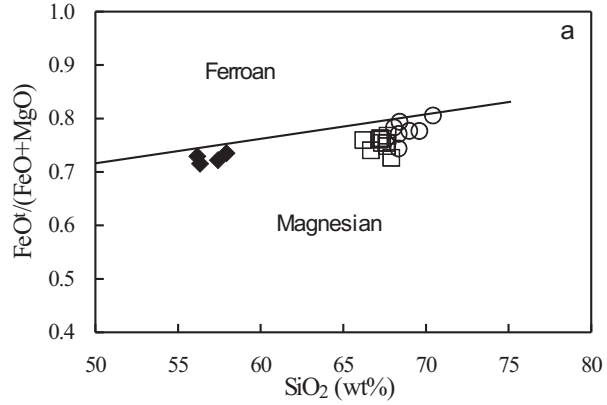


Figure 10. (a) $\text{FeO}'/(\text{FeO}' + \text{MgO})$ vs SiO_2 (wt%) diagram and (b) $(\text{Na}_2\text{O} + \text{K}_2\text{O} - \text{CaO})$ vs SiO_2 (wt%) diagram (Frost *et al.* 2001). See Figure 3 for explanation.

Discussion

Petrogenetic Considerations

Petrogenetic models for the origin of subduction-related magmas are grouped into two broad categories: (1) they are interpreted to be derived from basaltic parent magmas by FC or assimilation and fractional crystallisation (AFC) processes (Bacon & Druitt 1988) or (2) they are regarded as products of lower crustal dehydration melting of mafic to intermediate metagneous (Rapp & Watson 1995; Singh & Johannes 1996) or metasedimentary (Patiño Douce & Beard 1996; Stevens *et al.* 1997) sources. The first model is thought unlikely, because the bulk of subduction-related volcanic and intrusive rocks is felsic rather than basaltic in the study area.

The Sariosman intrusions consist of abundant felsic magmas ($\text{SiO}_2 = 66\text{--}70$ wt%; $\text{Mg}\# = 19\text{--}27$,

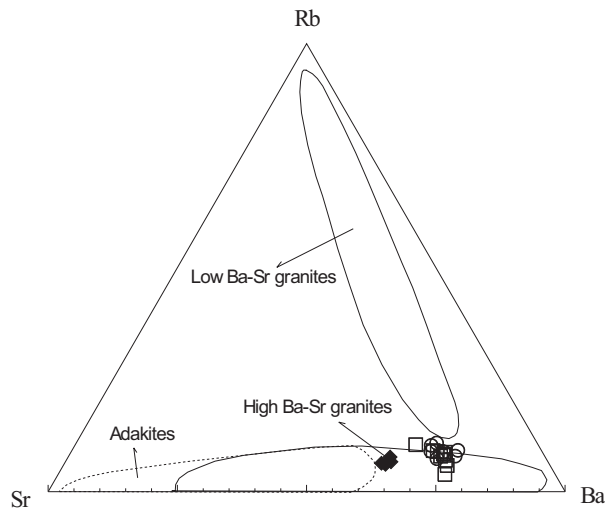


Figure 11. Sr-Rb-Ba plot (Tarney & Jones 1994) for samples from the Sariosman intrusions. See Figure 3 for explanation.

Table 7) and it is improbable that all these melts were generated by fractionation of mantle-derived mafic magmas. In the study area and adjacent regions, the rock compositions do not represent a fractionation sequence from basalt to monzogranite. If there was a single mafic magma source from which the felsic rocks were solidified through the FC process, the chondrite-normalised REE pattern of the felsic rocks should show a strong fractionation between the light and heavy REEs, with a pronounced negative Eu anomaly. These characteristics are not observed in the felsic rocks of the Sariosman pluton. A derivation of the Sariosman intrusive from mafic magmas through AFC processes can also be excluded because all rocks show little variation in their initial Sr-Nd isotope ratios with SiO_2 (Figure 16b, c); larger isotopic variability would be expected if such a process had taken place.

Partial melting of lower crustal metabasalts yields a variety of granitoids, whose compositions are controlled by the amount of H_2O (Tepper *et al.* 1993). Experimental studies have shown that amphibolites start to melt at relatively high temperatures (800 to 900 °C) and at pressures $< 1 \text{ GPa}$ under anhydrous conditions, whereas dehydration melting commences at temperatures as low as 750 °C at $\sim 1 \text{ GPa}$ (Wyllie & Wolf 1993; Wolf & Wyllie 1994; Lopéz & Castro 2001). The specific melt

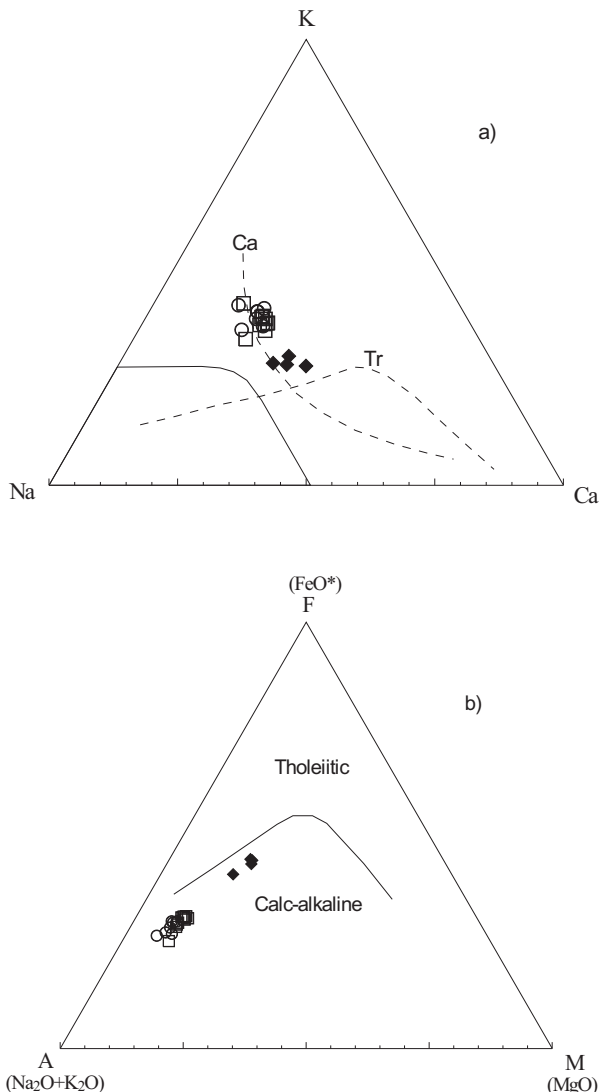


Figure 12. (a) Na-Ca-K ternary diagram and (b) AFM diagram (Irvine & Baragar 1971) showing tholeiitic to calc-alkaline trend for samples from the Sariosman intrusions. See Figure 3 for explanation.

composition resulting from the partial melting of the mafic lower crust is controlled by the water content, source composition, degree and the P-T conditions of the melting (Rapp *et al.* 1991; Sen & Dunn 1994; Wolf & Wyllie 1994; Rapp & Watson 1995; Winther 1996; Lopéz & Castro 2001). Using data obtained from partial-melting experiments on common crustal rocks, Roberts & Clemens (1993) stated that high-K, I-type, calc-alkaline granitoid magmas can be derived from partial melting of hydrous, calc-

Table 7. Whole-rock major- (wt%) and trace (ppm)-element analyses of representative samples and CIPW norms from the Sariosman intrusions.

Sample	Biotite hornblende monzogranite										Porphyritic hornblende biotite monzogranite										MME Qtz monzodiorite			
	A9	A19	A24	A20	A30	A27	A4	S3	A44	A16	A22	A40	A40a	S2	Sn10	P24	P25	P25	A4a	A4b				
SiO ₂	66.21	66.67	67.23	67.33	67.60	67.90	67.35	67.68	68.34	68.99	68.35	68.07	68.40	69.60	70.42	56.33	56.16	57.42	57.93					
TiO ₂	0.35	0.33	0.28	0.29	0.32	0.29	0.31	0.30	0.28	0.25	0.28	0.27	0.28	0.26	0.22	0.66	0.55	0.60	0.53					
Al ₂ O ₃	15.50	15.43	15.36	15.77	14.82	15.50	15.23	15.12	14.99	14.63	15.29	14.97	15.14	14.60	15.03	16.87	17.62	17.91	16.85					
Fe ₂ O ₃ ^T	3.89	3.74	3.74	3.41	3.84	3.03	3.94	3.84	3.08	3.17	3.54	3.65	3.70	3.27	3.15	8.02	7.49	7.33	7.05					
MnO	0.06	0.08	0.06	0.05	0.10	0.08	0.08	0.05	0.05	0.07	0.06	0.07	0.07	0.06	0.08	0.12	0.14	0.16	0.17					
MgO	1.23	1.31	1.16	1.11	1.25	1.14	1.23	1.16	1.06	0.91	1.05	1.01	0.96	0.94	0.76	3.19	2.78	2.82	2.54					
CaO	3.24	3.44	3.28	3.28	3.39	3.40	3.14	2.95	2.89	3.30	2.96	2.86	2.92	2.31	5.32	5.65	4.53	4.91						
Na ₂ O	3.20	3.13	3.03	3.04	3.02	3.16	3.90	3.07	2.84	3.05	3.11	3.10	3.56	3.07	3.29	3.62	3.13	3.03	3.88					
K ₂ O	4.26	4.06	4.17	4.39	4.26	4.69	4.28	4.42	4.47	4.51	4.16	4.59	4.18	4.24	4.70	3.70	3.47	3.43	3.78					
P ₂ O ₅	0.14	0.10	0.10	0.09	0.10	0.08	0.09	0.08	0.10	0.09	0.09	0.08	0.12	0.08	0.06	0.21	0.27	0.28	0.19					
LOI	1.30	1.40	1.00	0.70	1.20	1.20	0.00	0.90	1.30	0.90	0.50	1.00	0.50	0.70	0.50	1.70	2.40	2.20	2.16					
Total	99.4	99.7	99.4	99.5	99.9	99.5	99.8	99.8	99.5	99.5	99.7	99.8	99.8	99.7	100.5	99.7	99.7	99.7	99.9					
Ni	20.0	23.0	20.0	5.0	20.0	5.3	5.4	20.0	20.0	20.0	5.4	4.4	3.7	6.0	4.5	1.0	2.2	2.2	4.4					
V	62	64	65	60	67	53	63	61	59	57	53	53	43	51	52	190	146	148	146					
Cu	4.4	5.2	9.1	18.0	10.3	9.8	8.1	23.7	7.2	18.1	3.2	11.1	21.0	3.9	5.7	54.0	28.2	28.9	32.5					
Pb	4.50	16.50	6.60	7.90	7.60	16.90	8.10	9.40	5.50	15.30	4.60	8.80	9.10	7.50	16.50	10.20	4.40	4.40	3.40	5.49				
Zn	23.0	19.0	19.0	14.0	16.0	33.0	16.0	17.0	50.0	17.0	14.0	15.0	18.0	90.0	20.0	18.0	168.0	129.0	118.0					
W	1.30	2.10	2.00	1.90	2.60	4.90	3.80	3.20	2.70	24.30	1.50	2.90	5.50	2.20	3.80	1.70	16.50	5.50	3.20					
Rb	93	122	114	141	135	155	129	138	143	155	113	143	135	123	147	97	107	98	113					
Ba	1815	1275	1444	1210	1071	972	1176	1138	1153	993	1095	1344	898	943	1190	992	1037	921	905					
Sr	518	341	387	323	306	349	329	295	304	277	323	311	270	291	257	505	547	444	436					
Ta	0.30	0.80	1.00	0.80	0.80	1.00	1.00	1.00	1.00	0.60	1.10	1.00	1.30	1.10	0.80	0.60	1.50	1.10	1.30					
Nb	7.30	9.30	10.60	10.40	9.30	11.00	10.80	9.90	10.90	9.30	11.10	10.60	13.50	11.10	13.60	7.60	15.90	15.60	11.40					
Hf	3.70	4.70	4.30	4.70	4.10	4.20	4.20	4.10	4.40	3.50	4.20	4.50	5.60	3.50	4.50	3.10	4.40	4.70	4.65					
Zr	131	160	141	136	138	131	142	147	129	120	139	138	172	111	139	88	128	160	153					
Ti	2088	1969	1671	1730	1909	1730	1850	1790	1671	1492	1671	1611	1671	1551	1313	3938	3281	3580	3162					
Y	16.00	16.50	18.90	17.10	15.70	16.40	17.10	17.00	18.30	16.50	16.40	16.20	16.70	15.80	18.60	20.20	29.00	26.80	25.40					

Table 7. Continued.

Sample	Biotite hornblende monzogranite						Porphyritic hornblende biotite monzogranite						MME Qtz monzodiorite						
	A9	A19	A24	A20	A30	A27	A4	S3	A44	A16	A22	A40	A40a	S2	Sn10	P24	P25	A4a	A4b
Th	19.00	25.20	29.70	26.40	20.70	28.50	29.30	30.80	31.30	37.20	28.00	30.10	33.20	37.60	15.30	22.60	22.10	23.40	
U	4.10	5.60	4.30	4.90	2.90	3.90	4.30	4.30	2.30	3.60	4.50	4.00	8.00	3.60	5.00	2.50	3.20	2.40	2.30
Ga	16.60	13.30	16.90	16.40	12.60	16.60	13.00	12.60	16.90	17.10	12.80	12.50	11.70	14.80	15.90	16.30	16.40	15.60	
Q	20.64	22.00	23.01	22.45	23.36	23.27	18.45	22.83	25.31	25.22	24.20	23.02	22.76	26.51	25.50	3.48	6.39	10.28	5.25
Or	26.63	25.01	25.80	26.96	26.05	28.51	26.24	27.06	27.36	27.45	25.46	28.21	25.43	25.86	28.72	22.66	21.38	21.00	23.06
Ab	27.08	26.49	25.64	25.72	25.55	26.74	33.00	25.98	24.03	25.81	26.32	26.23	30.12	25.98	27.84	30.63	26.49	25.64	32.83
An	14.62	15.55	15.41	15.79	13.86	11.44	10.94	13.95	14.09	12.51	15.04	12.83	12.62	13.13	11.18	18.45	23.34	20.78	17.03
Di	0.58	0.80	0.28	0.00	1.99	0.00	4.52	0.98	0.00	1.10	0.71	1.20	0.72	0.76	0.00	5.53	2.54	0.00	5.13
Hy	5.84	5.88	5.82	5.48	5.24	5.30	4.04	5.55	5.07	4.33	5.13	4.92	5.06	4.62	4.53	11.64	11.83	13.00	9.63
Ol	0.00	0.00	0.00	0.00	0.00	0.00	0.00	0.00	0.00	0.00	0.00	0.00	0.00	0.00	0.00	0.00	0.00	0.00	0.00
Co	0.00	0.00	0.04	0.00	0.89	0.00	0.00	0.00	0.14	0.00	0.00	0.00	0.00	0.00	0.00	0.26	0.00	0.00	1.46
Sph	0.00	0.00	0.00	0.00	0.00	0.00	0.00	0.00	0.00	0.00	0.00	0.00	0.00	0.00	0.00	0.00	0.00	0.00	0.00
Zr	0.03	0.03	0.03	0.03	0.03	0.03	0.03	0.03	0.03	0.03	0.03	0.03	0.03	0.03	0.03	0.01	0.03	0.03	0.03
Ap	0.32	0.23	0.23	0.21	0.23	0.19	0.21	0.19	0.23	0.21	0.21	0.21	0.19	0.28	0.19	0.14	0.49	0.63	0.65
Ilm	0.66	0.63	0.53	0.55	0.61	0.55	0.59	0.57	0.53	0.47	0.53	0.51	0.53	0.49	0.42	1.25	1.04	1.14	1.01
Ru	0.00	0.00	0.00	0.00	0.00	0.00	0.00	0.00	0.00	0.00	0.00	0.00	0.00	0.00	0.00	0.00	0.00	0.00	0.00
Ma	1.70	1.62	1.62	1.48	1.67	1.32	1.71	1.67	1.33	1.38	1.54	1.59	1.61	1.42	1.38	3.49	3.26	3.19	3.07
Mg [#]	24.0	25.9	23.7	24.6	24.6	27.3	23.8	23.2	25.6	22.3	22.9	21.7	20.6	22.3	19.4	28.5	27.1	27.8	26.49
ASI	0.98	0.98	1.00	0.94	1.06	0.88	0.97	1.01	0.97	0.98	0.97	0.97	0.98	1.02	0.86	0.92	1.06	0.87	
K/Na	1.33	1.30	1.38	1.44	1.41	1.48	1.10	1.44	1.57	1.48	1.34	1.48	1.17	1.38	1.43	1.02	1.11	1.13	0.97
Rb/Sr	0.18	0.36	0.29	0.44	0.44	0.44	0.39	0.47	0.47	0.56	0.35	0.46	0.50	0.42	0.57	0.19	0.20	0.22	0.26
K/Rb	380	276	304	259	261	252	275	265	260	242	307	267	258	287	265	316	268	292	279
Sr/Y	32.35	20.68	20.46	18.90	19.51	21.29	19.22	17.32	16.62	16.76	19.70	19.18	16.17	18.44	13.82	25.01	18.87	16.55	17.15
K/Ti	16.94	17.12	20.72	21.06	18.52	22.50	19.21	20.50	22.21	25.10	20.67	23.65	20.77	22.69	29.73	7.80	8.78	7.95	9.92
Th/Zr	15.98	12.28	11.86	12.72	13.81	13.24	13.03	12.22	12.97	12.48	12.05	11.69	9.71	14.00	9.42	44.90	25.68	22.32	20.61

$Fe_2O_3^{T}$ is total iron as Fe_2O_3 , LOI is loss on ignition, Mg# (mg-number) = $100 \times MgO / (MgO + Fe_2O_3)$, ASI = molar $Al_2O_3 / (CaO + Na_2O + K_2O)$, MME = mafic microgranular enclaves, Qtz = quartz

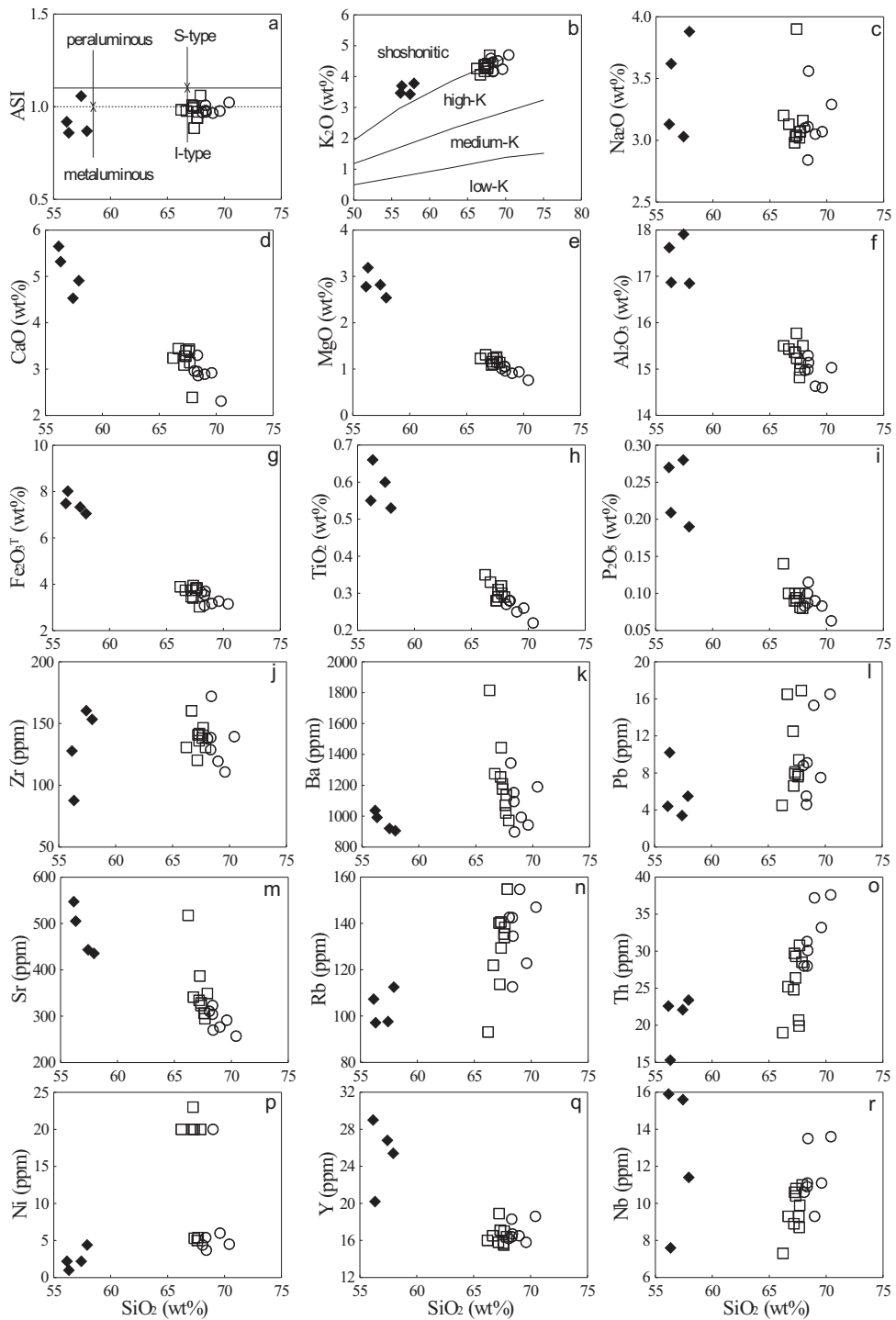


Figure 13. Variation diagrams of SiO_2 (wt%) versus major oxides (wt%) and trace elements (ppm) for samples from the Sariosman intrusions. (a) ASI vs SiO_2 , with field boundaries between I-type and S-type, according to Chappell & White (1974) and peraluminous and metaluminous fields of Shand (1947). (b) K_2O vs SiO_2 diagram with field boundaries between medium-K, high-K and shoshonitic series according to Peccerillo & Taylor (1976). ASI (aluminium saturation index) = molar $\text{Al}_2\text{O}_3/(\text{Na}_2\text{O}+\text{K}_2\text{O}+\text{CaO})$. See Figure 3 for explanation.

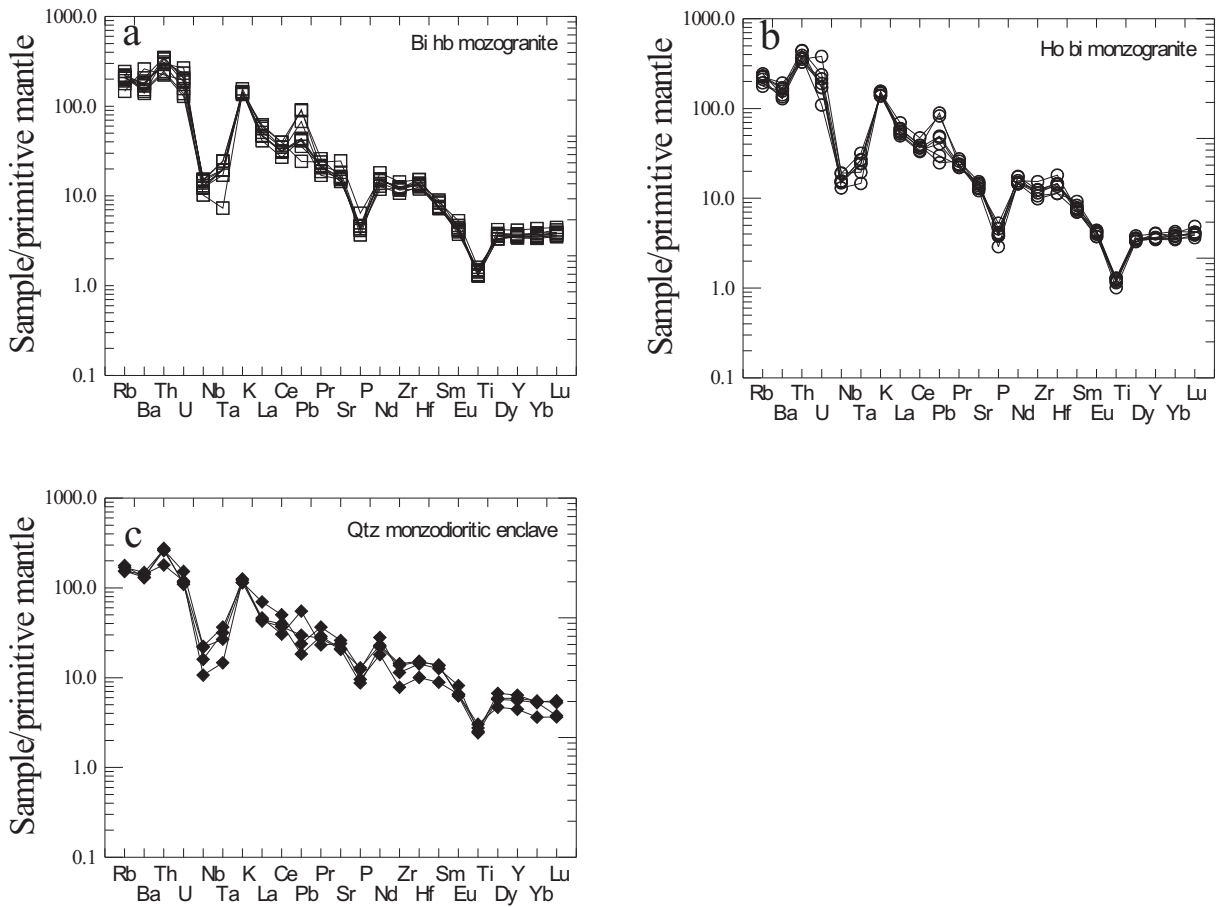


Figure 14. Primitive mantle-normalised trace-element patterns (normalising values from Sun & McDonough 1989) for samples from the Sariosman intrusions. See Figure 3 for explanation.

alkaline mafic to intermediate metamorphic rocks. Recent experimental data have also shown that partial melting of the mafic lower crust can generate melts of metaluminous granitic composition and that the melt composition is largely independent of the degree of partial melting (Rushmer 1991; Tepper *et al.* 1993; Roberts & Clemens 1993; Wolf & Wyllie 1994; Rapp & Watson 1995).

The MMEs in the eastern part of the Sariosman pluton suggest limited mingling between small volumes of monzodioritic magma and coexisting monzogranitic magma. MMEs and host granitoids show similar mineral assemblages, mineral compositions and strong correlations between major

and trace elements, although the concentration ranges of major and trace elements are different within each rock type. Oscillatory-zoned plagioclases, coexistence of two types of plagioclase phenocrysts, poikilitic textures (Figure 4b, d and e), acicular hornblende, biotite and apatite, and K-feldspar megacrysts in mafic microgranular enclaves (Barbarin 1988; Lesher 1990; Hibbard 1991; Baxter & Feely 2002) possibly record the mixing of coexisting mafic and felsic magmas. Because the original compositions of the enclaves (former globules of mafic melt) were probably modified by interaction with the felsic host magma, a more thorough discussion of the genesis of the microgranular enclaves is beyond the scope of this study.

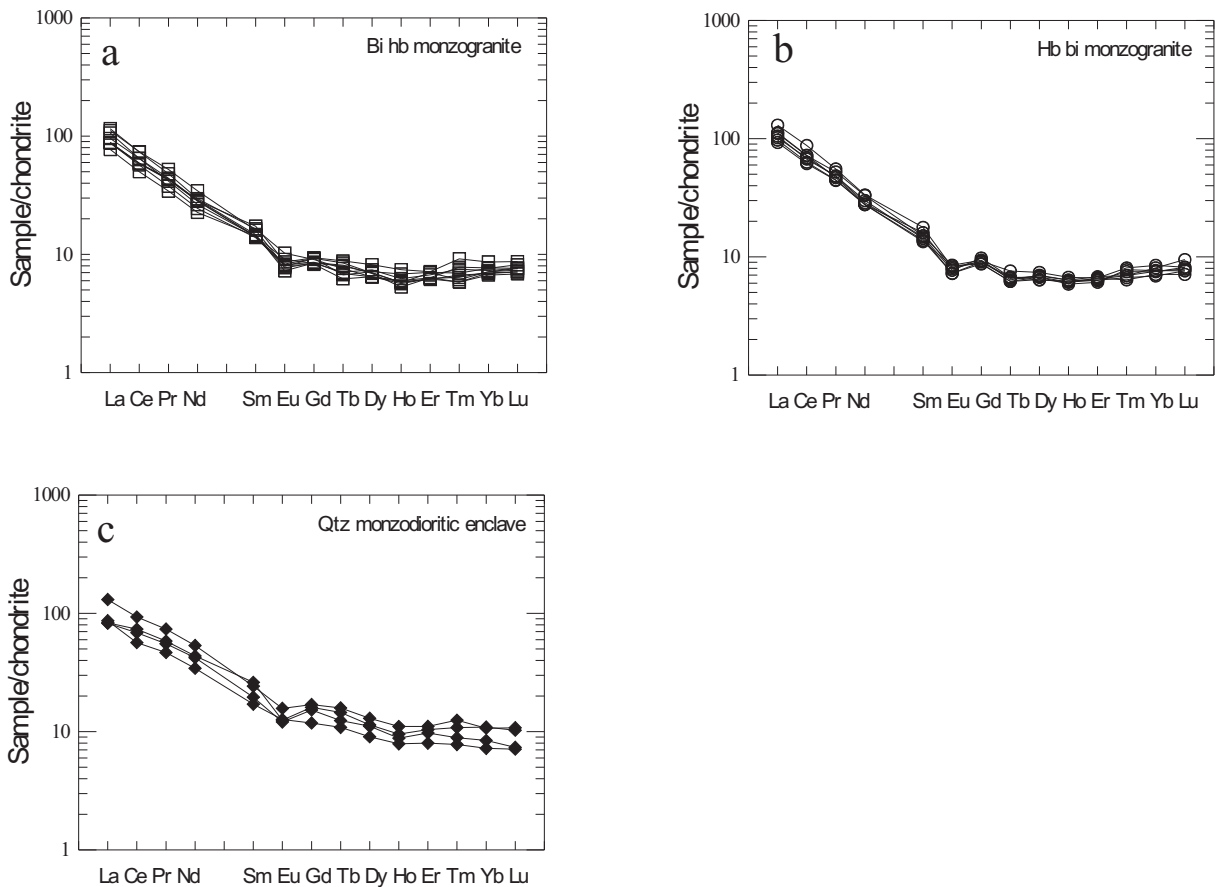


Figure 15. Chondrite normalised rare earth–element patterns (normalising values from Taylor & McLennan 1985) for samples from the Sariosman intrusions. See Figure 3 for explanation.

FC Process in Evolution

In variation diagrams (Figures 14 & 15), CaO, MgO, Fe₂O₃, Al₂O₃, TiO₂, P₂O₅, Sr and Y increase, whereas K₂O and Rb decrease with increasing silica, which is compatible with their evolution through FC processes in the Sariosman samples. This is well supported by the depletion in Sr, Ba, P and Eu (Figure 14). Negative Eu anomalies (Figure 15) require fractionation of plagioclase and/or K-feldspar. Fractionation of feldspar would also result in depletion of Ba and Sr. Negative Eu anomalies and a decrease of Sr with increasing silica (Figure 13m) establish that plagioclase was an important fractionating phase. The rocks show similar REE patterns, with a general increase of both the light and the heavy REE with increasing SiO₂ (Figure 15). The magnitude of the negative chondrite-normalised Eu

anomalies increases with increasing SiO₂ contents, suggesting fractionation of plagioclase for both sub-intrusions. Depletion in P results from removal of apatite during FC. The increase of K₂O and Rb with increasing silica indicates that K-feldspar and biotite are not early fractionation phases. This is in accordance with the late appearance of both minerals in the crystallisation sequence. All the variation trends of the major and trace elements bear evidence that fractionation of plagioclase, hornblende, apatite and titanite occurred during the formation of the Sariosman intrusions.

Source Rocks of the Sariosman Intrusion

The geochemical features of the Sariosman intrusions (i.e. depletion of Nb, Ba, Sr and Ti;

Table 8. Rare earth-element analyses (ppm) from the Sarıosman intrusions.

ppm	Biotite hornblende monzogranite						Porphyritic hornblende biotite monzogranite						MME Qtz monzodiorite							
	A9	A19	A24	A20	A30	A27	A4	S3	A44	A16	A22	A40	A40a	S2	Sn10	P24	P25	A4a	A44	
La	42.50	40.90	35.10	28.30	32.40	39.00	32.40	48.80	41.20	47.70	40.50	34.10	38.60	35.70	37.40	31.80	48.00	30.50	30.30	
Ce	70.30	70.60	62.00	47.90	56.50	62.10	56.40	82.20	69.20	83.70	68.90	58.90	64.30	60.60	65.90	54.10	89.10	70.30	65.70	
Pr	6.58	7.17	6.04	4.69	5.90	5.69	5.98	8.44	6.41	7.59	7.16	6.08	6.62	6.12	6.59	6.39	10.10	7.98	7.56	
Nd	21.00	24.50	20.30	16.10	20.50	18.70	20.00	27.30	19.70	23.70	23.50	19.70	21.30	19.70	20.40	24.40	38.00	31.00	30.00	
Sm	3.80	3.70	4.00	3.30	3.40	3.30	3.27	3.89	3.70	4.10	3.49	3.11	3.31	3.19	3.41	3.94	5.60	6.03	4.52	
Eu	0.89	0.69	0.75	0.79	0.63	0.71	0.72	0.74	0.69	0.71	0.74	0.73	0.63	0.63	0.67	1.10	1.37	1.09	1.05	
Gd	2.77	2.83	2.86	2.57	2.59	2.63	2.83	2.94	2.82	2.79	2.87	2.67	2.77	2.67	2.99	3.62	5.19	4.91	4.67	
Tb	0.44	0.49	0.51	0.41	0.46	0.40	0.39	0.39	0.44	0.39	0.37	0.37	0.36	0.38	0.36	0.39	0.63	0.92	0.84	0.72
Dy	2.45	2.65	3.11	2.82	2.67	2.46	2.72	2.74	2.81	2.56	2.66	2.45	2.63	2.57	2.43	3.45	4.94	4.35	4.23	
Ho	0.50	0.49	0.63	0.53	0.49	0.51	0.58	0.58	0.57	0.50	0.54	0.52	0.54	0.52	0.53	0.67	0.94	0.81	0.75	
Er	1.53	1.74	1.78	1.67	1.54	1.58	1.75	1.73	1.65	1.52	1.57	1.64	1.69	1.58	1.61	1.99	2.76	2.59	2.43	
Tm	0.24	0.22	0.33	0.27	0.21	0.28	0.25	0.26	0.29	0.28	0.27	0.23	0.25	0.24	0.25	0.28	0.45	0.39	0.32	
Yb	1.71	1.77	2.14	1.81	1.73	1.91	1.89	1.79	2.10	1.90	1.86	1.76	2.00	1.71	1.87	1.79	2.65	2.71	2.09	
Lu	0.27	0.28	0.33	0.29	0.27	0.29	0.31	0.29	0.31	0.29	0.31	0.27	0.36	0.29	0.30	0.27	0.41	0.39	0.28	
(La/Lu) _{en}	16.30	15.12	11.01	10.10	12.43	13.92	10.82	17.42	13.76	17.03	13.53	13.08	11.10	12.75	12.91	12.19	12.12	8.10	10.83	
(La/Sn) _{en}	7.04	6.96	5.52	5.40	6.00	7.44	6.24	7.90	7.01	7.32	7.30	6.90	7.34	7.04	6.90	5.08	5.40	3.18	2.99	
(Gd/Lu) _{en}	1.27	1.26	1.08	1.10	1.19	1.13	1.13	1.26	1.13	1.19	1.15	1.23	0.96	1.14	1.24	1.66	1.57	1.56	2.07	
(La/Yb) _{en}	16.79	15.61	11.08	10.57	12.66	13.80	11.58	18.42	13.26	16.96	14.71	13.09	13.04	14.11	13.51	12.00	12.24	7.61	7.64	
(Tb/Yb) _{en}	1.10	1.18	1.02	0.97	1.14	0.90	0.88	0.93	0.90	0.88	0.85	0.87	0.81	0.90	0.89	1.50	1.48	1.33	1.19	
Eu/Eu*	0.80	0.63	0.65	0.80	0.62	0.71	0.71	0.64	0.63	0.61	0.69	0.76	0.62	0.64	0.63	0.88	0.76	0.59	0.58	

Eu*=(Sm+Gd)_{en}/2, MME= mafic microgranular enclaves, Qtz= quartz

Table 9. Rb-Sr and Sm-Nd isotope data from the Sarosman intrusions.

Sample	Rb (ppm)	Sr (ppm)	$^{87}\text{Rb}/^{86}\text{Sr}$	$^{87}\text{Sr}/^{86}\text{Sr}$	2σm	$(^{87}\text{Sr}/^{86}\text{Sr})_{\text{SM}}$	Sm (ppm)	Nd (ppm)	$^{147}\text{Sm}/^{144}\text{Nd}$	$^{147}\text{Nd}/^{144}\text{Nd}$	2cm	$(^{147}\text{Nd}/^{144}\text{Nd})_{\text{SM}}$	$\epsilon_{\text{Nd}}(0)^{\text{a}}$	$\epsilon_{\text{Nd}}(\text{i})^{\text{a}}$	$\epsilon_{\text{Nd}}(0)^{\text{a}}$	T_{DM}^{b}	T_{DM}^{c}
Biotite hornblende monzogranite																	
A9	116.00	342.90	0.97876	0.70741	12	0.70627	3.16	17.61	0.10837	0.51244	11	0.51238	-2.97	-3.90	0.98	1.13	
H38	128.62	321.65	1.15696	0.70757	12	0.70622	3.19	18.59	0.10365	0.51242	12	0.51237	-3.19	-4.16	0.96	1.14	
A19	102.42	372.16	0.79623	0.70735	13	0.70643	3.43	20.88	0.09938	0.51243	11	0.51238	-3.05	-4.07	0.92	1.13	
Porphyritic hornblende biotite monzogranite																	
A16	134.32	310.44	1.25184	0.70778	14	0.70632	3.41	19.81	0.10402	0.51242	13	0.51237	-3.22	-4.19	0.96	1.15	
A40	90.41	474.65	0.55108	0.70766	14	0.70702	3.78	22.99	0.09931	0.51238	12	0.51232	-4.10	-5.11	0.99	1.22	

^a $\epsilon_{\text{Nd}}(\text{i})$ and $\epsilon_{\text{Nd}}(0)$ values are calculated based on present-day $^{147}\text{Sm}/^{144}\text{Nd} = 0.1967$ and $^{143}\text{Nd}/^{144}\text{Nd} = 0.512638$ ^b Single stage model age (T_{DM}), calculated with depleted mantle present-day parameters $^{143}\text{Nd}/^{144}\text{Nd} = 0.513151$ and $^{147}\text{Sm}/^{144}\text{Nd} = 0.219$ ^c Two-stage model age (T_{DM}), according to Liew & Hofman (1988)

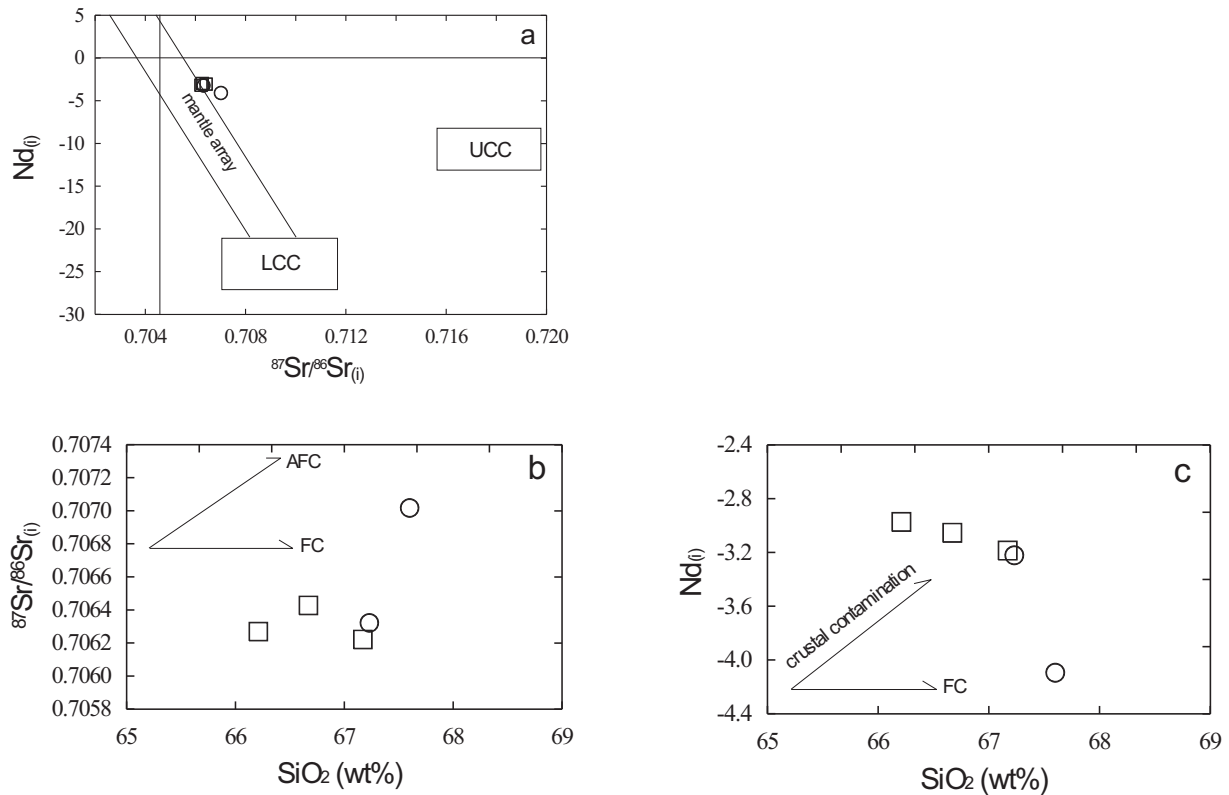


Figure 16. (a) $\epsilon_{\text{Nd(i)}}$ values vs $^{87}\text{Sr}/^{86}\text{Sr}_{(i)}$ ratio; (b) and (c) $^{87}\text{Sr}/^{86}\text{Sr}_{(i)}$ and $\epsilon_{\text{Nd(i)}}$ vs SiO₂, respectively. $\epsilon_{\text{Nd(i)}}$ and $^{87}\text{Sr}/^{86}\text{Sr}_{(i)}$ values are calculated for an age of 82 Ma. See Figure 3 for explanation.

enrichment of K, Rb, Th, Pb and LREEs) are compatible with those of typical crustal melts, such as the granitoids of the Lachlan Fold belt (Chappell & White 1992). Several experimental studies (Wolf & Wyllie 1994; Rapp & Watson 1995) have shown that extremely high temperatures in excess of ~1100 °C are needed to produce mafic metaluminous low-silica (~58 wt%) melts by dehydration melting of metabasic crustal rocks. Compositional diversity among the crustal magmas may arise, in part, from different source compositions: nevertheless, variations of intrinsic parameters, such as temperature, pressure, oxygen fugacity, or water content during partial melting also play an equally important role (Beard *et al.* 1994; Wolf & Wyllie 1994; Patiño Douce & Beard 1996; Thompson 1996; Stevens *et al.* 1997; Altherr *et al.* 2000). These parameters control the degree of partial melting and

the stability fields of the residual mineral phases (plagioclase, biotite, hornblende, orthopyroxene and garnet) that buffer the resultant melt composition. Compositional differences of magmas produced by partial melting of different source rocks, such as amphibolites, tonalitic gneisses, metagreywackes and metapelites, under variable melting conditions, may be visualised in terms of molar oxide ratios. Dehydration melting of metapelites and metagreywackes (Rapp *et al.* 1991; Rapp 1995; Rapp & Watson 1995) yields higher values for Mg#, K₂O/Na₂O, (Na₂O+K₂O)/(FeO^T+MgO+TiO₂) and Al₂O₃/(FeO^T+MgO+TiO₂) and lower CaO+FeO^T+MgO+TiO₂ values, compared to the investigated rocks (Figure 17). The chemical compositions of the Sarıosman intrusions are thus broadly compatible with an origin by dehydration melting from mafic lower crustal rocks.

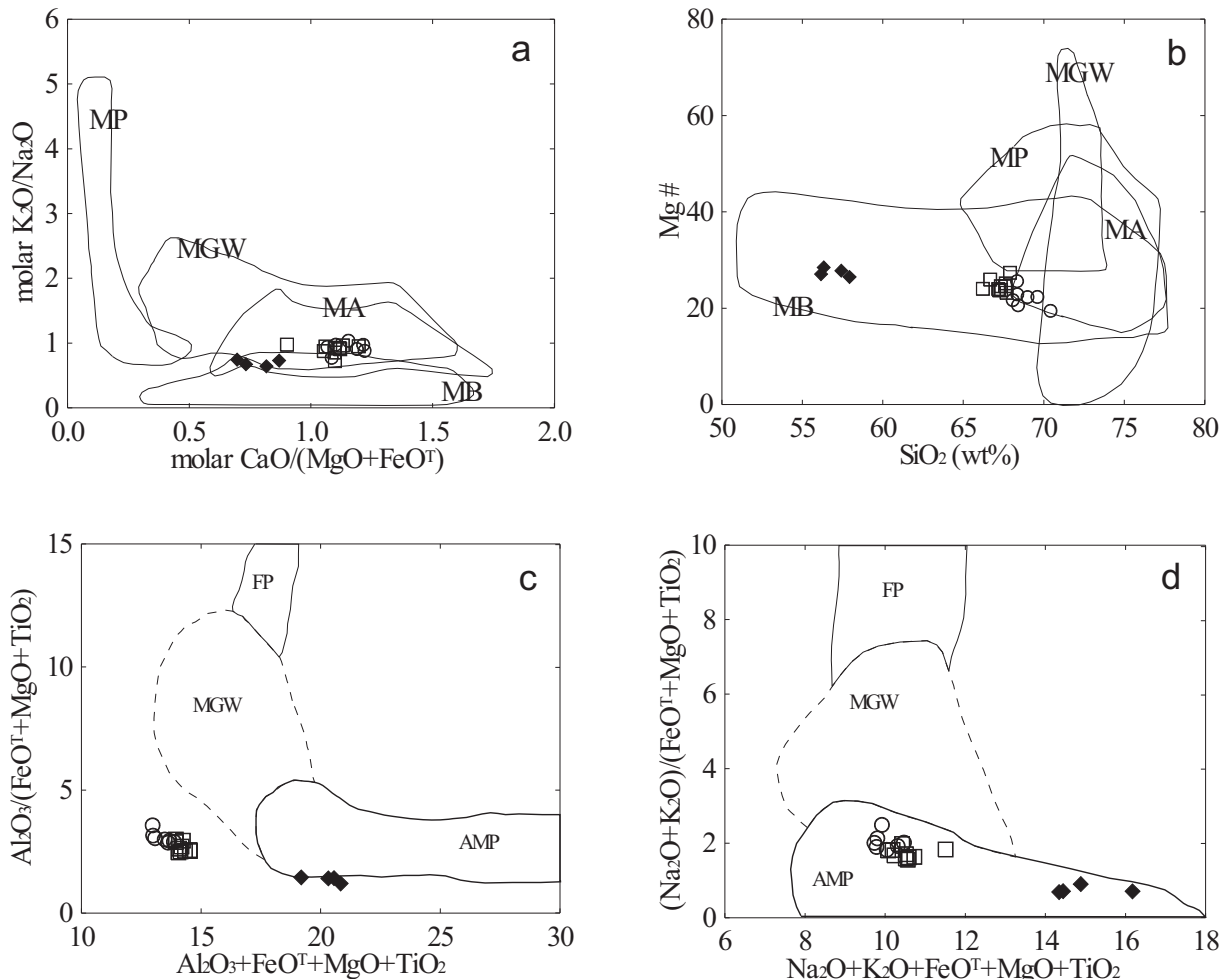


Figure 17. Chemical composition of the Sariosman intrusions: Outlined fields denote compositions of partial melts obtained in experimental studies by dehydration melting of various bulk compositions. MB- metabasalts (bold-solid line); MA- metaandesites (dotted line); MGW- metagreywackes (dashed line); MP- metapelites (solid line); AMP- amphibolites (bold-solid line). Data sources: Vielzeuf & Holloway (1988), Patiño Douce & Johnston (1991), Rapp *et al.* (1991), Gardien *et al.* (1995), Rapp (1995), Rapp & Watson (1995), Patiño Douce & Beard (1996), Stevens *et al.* (1997), Skjerlie & Johnston (1996), Patiño Douce (1997, 1999), Patiño Douce & McCarthy (1998). See Figure 3 for explanation.

Emplacement and Tectonic Implications

The Sariosman intrusions comprise the elliptical pluton, and the contacts between the Sariosman intrusions and the country rocks are dominantly sharp and discordant. The contact facies are finer-grained, and the textures are massive, porphyritic and granophyric. The intrusion contains abundant country-rock xenoliths near the margin. All these

features show that the Sariosman pluton was emplaced at shallow crustal depth either by a stoping type of ascent or by ballooning.

Gedikoğlu (1978) has proved that subduction-related fracture tectonics played an important role during the emplacement of the granitoids within the Pontide magmatic arc. The long axes of most granitic plutons are usually aligned with the major NE-SW

or NW-SE tectonic directions, which correspond to the two main fracture alignments in the Eastern Pontides defined by Bektaş & Çapkinoğlu (1997). They suggest the important role of fractures during pluton emplacement. It therefore appears probable that the Sarıosman intrusions were emplaced along a NE-SW-trending fracture line during the Late Cretaceous.

The Sarıosman intrusions comprise high-K, calc-alkaline rocks, enriched in LILE (Rb, Ba and K) and depleted in the HFSE (Nb and Ti), and introduce significant positive Pb anomalies (Figures 13–15). Magmas with these chemical features are generally believed to be generated in subduction-related environments (Floyd & Winchester 1975; Rogers & Hawkesworth 1989; Sajona *et al.* 1996).

In a FeO^T/MgO – $(\text{Zr}+\text{Nb}+\text{Ce}+\text{Y})$ tectonic-discrimination diagram (Whalen *et al.* 1987), all the samples are grouped within the I-type granite field (Figure 18a). The $(\text{Zr}+\text{Nb}+\text{Ce}+\text{Y})$ – $(\text{K}_2\text{O}+\text{Na}_2\text{O})/\text{CaO}$ diagram (not shown here) yields the same results. Applying the discrimination criteria of Pearce *et al.* (1984), all samples plot in the fields of volcanic-arc granites (VAG) and syncollisional granites in the Nb-Y diagram (Figure 18b), whereas in the Rb-(Y+Nb) diagram, the samples plot in the VAG field (Figure 18c). Difficulties exist in discriminating between collisional and arc-type granitoids (Brown *et al.* 1984; Pearce *et al.* 1984). Rb-Hf-Ta ratios of granitoids are used to separate collision-zone from arc setting magmatism (Harris *et al.* 1986). The Rb/30–Hf-Ta³ ternary diagram of Harris *et al.* (1986) provides a better distinction between volcanic-arc granites and pre-syn-late collisional granites. The Sarıosman samples plot in the VAG field of this diagram (Figure 18d). In the Rb/Zr-SiO₂ and Ta-Nb diagrams (Harris *et al.* 1986) (not shown here), the Sarıosman intrusions share similar characteristics with volcanic-arc granitoids.

Brown *et al.* (1984) established that the abundances of incompatible elements in granites can be correlated with the degree of arc maturity. Increasing Nb and Y content with increasing Rb/Zr ratios is in accordance with the arc maturity, from primitive to mature. A comparison of the Sarıosman intrusion with the arc-type granitoids is presented on a Nb-Rb/Zr diagram (Figure 18e). All rock types

from the pluton plot in the normal arc fields (Figure 18e). On the Sr/Y-Y diagram (Figure 18f), all samples plot in the low Sr/Y and high Y areas, similar to samples from modern island-arcs. The $(\text{La}/\text{Yb})_n$ – Yb_n diagram (not shown) yields the same results.

Volcanic-arc granitoids, related to the subduction of Neotethys, occur in other parts of the Pontide belt (Arslan *et al.* 2004; Karslı *et al.* 2004; Boztuğ *et al.* 2004; Yılmaz-Şahin 2005; Boztuğ 2008; İlbeli 2008; Kaygusuz *et al.* 2008; Kaygusuz & Aydinçakır 2009) and further east along the Neotethyan belt: a similar history of intra-oceanic accretion and later marginal-arc magmatism of Cretaceous age is recorded in the Kohistan-Karakorum-Himalayas area (Crawford & Searle 1992; Debon *et al.* 1987; Petterson & Windley 1985; Rolland *et al.* 2002).

Conclusions

The Sarıosman pluton, containing biotite-hornblende monzogranite and minor porphyritic hornblende-biotite monzogranite, is considered a part of the Late Cretaceous arc-related igneous activity at an active continental margin. U-Pb SHRIMP zircon dating of biotite-hornblende monzogranite yielded an emplacement age of 82.7 ± 1.5 Ma.

The Sarıosman pluton has subalkaline affinity and belongs to the high-K, calc-alkaline and I-type character group. The intrusions display concave upward chondrite-normalised REE patterns with pronounced negative Eu anomalies. All rock types of the pluton show a small range of Sr-Nd values (initial $^{87}\text{Sr}/^{86}\text{Sr}$ = from 0.7062 to 0.707; $\varepsilon_{\text{Nd(i)}}$ = from -3.0 to -4.1). All these characteristics, combined with the low values of $\text{K}_2\text{O}/\text{Na}_2\text{O}$, Mg-number and ratios of $\text{Al}_2\text{O}_3/(\text{FeO}^T+\text{MgO}+\text{TiO}_2)$ and $(\text{Na}_2\text{O}+\text{K}_2\text{O})/(\text{FeO}^T+\text{MgO}+\text{TiO}_2)$, suggest an origin by dehydration melting from a metabasaltic lower crustal source.

The regional, geological and tectonic settings confirm that the Sarıosman pluton was emplaced in an arc-related geodynamic regime during subduction of the Neotethyan Ocean beneath the Eurasian plate along the İzmir-Ankara-Erzincan suture zone in Late Cretaceous times.

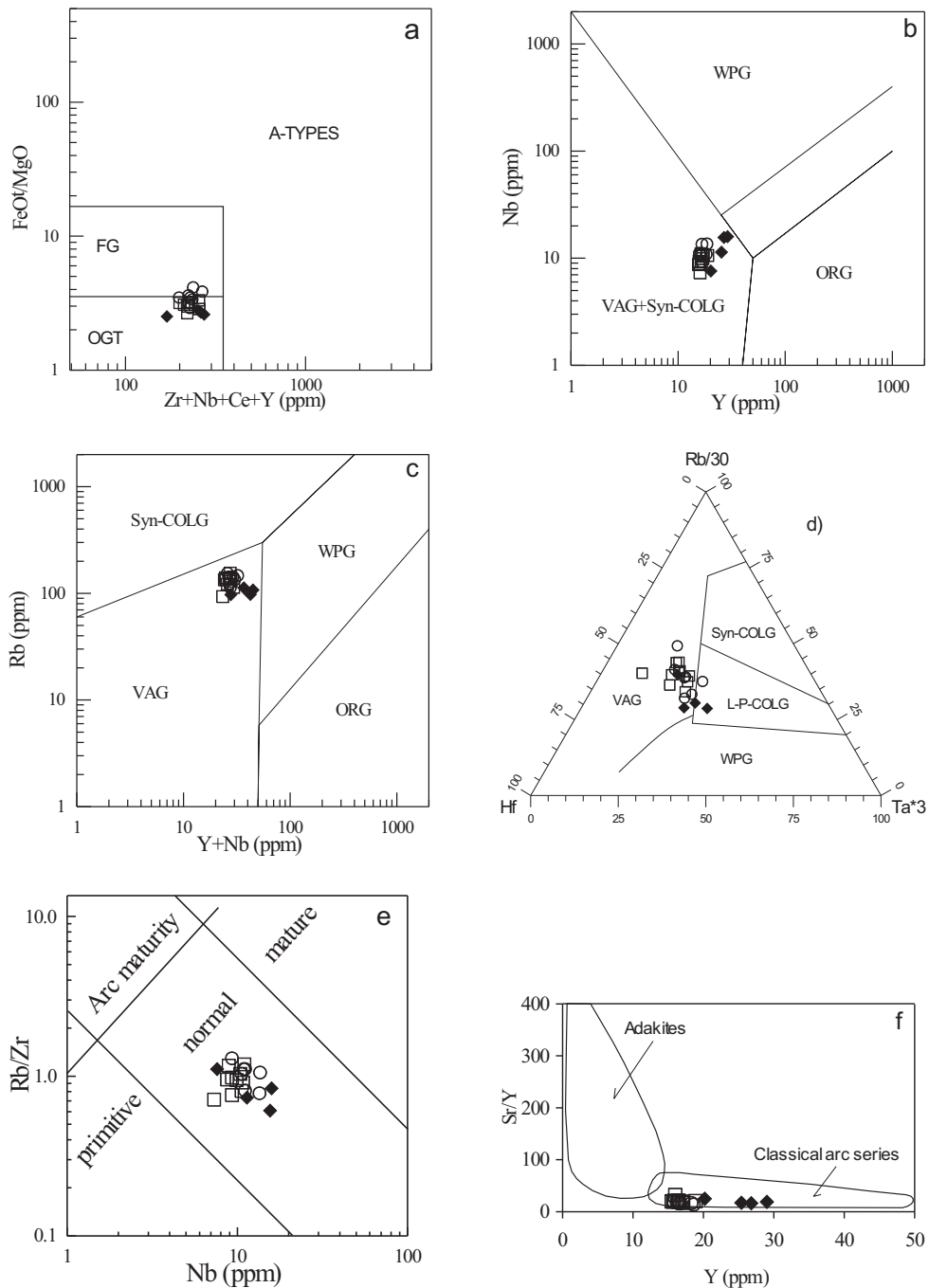


Figure 18. (a) FeO^*/MgO – ($\text{Zr}+\text{Nb}+\text{Ce}+\text{Y}$) classification diagram (Whalen *et al.* 1987), (b, c) $\text{Nb}-\text{Y}$ and $\text{Rb}-(\text{Y}+\text{Nb})$ discrimination diagrams, respectively (Pearce *et al.* 1984), (d) $\text{Rb}/30-\text{Hf}-\text{Ta}^*3$ triangular diagram (Harris *et al.* 1986), (e) $\text{Nb}-\text{Rb}/\text{Zr}$ diagram (Brown *et al.* 1984), (f) $\text{Sr}/\text{Y}-\text{Y}$ for samples from the Sariosman intrusions. Adakites and island-arc fields are adopted from Drummond & Defant (1990). FG – fractionated granitoid; OGT – unfractionated; VAG – volcanic-arc granites; Syn-COLG – syncollisional granites; WPG – within-plate granites; ORG – ocean-ridge granites; L-P-COLG – late-post collisional granites. See Figure 3 for explanation.

Acknowledgements

This work was supported by the Research Fund of Karadeniz Technical University. Thanks are extended to Ellery Frahm for microprobe analyses. Erdin Bozkurt and anonymous reviewers are kindly

thanked for their general improvement of the manuscript. Emre Aydinçakır is thanked for his enthusiastic assistance during fieldwork. John A. Winchester edited the English of the final text.

References

- ABDEL-RAHMAN, A.F.M. 1994. Nature of biotites from alkaline, calc-alkaline and peraluminous magmas. *Journal of Petrology* **35**, 525–541.
- ADAMIA, S.A., LORDKIPANIDZE, M.B. & ZAKARIADZE G.S. 1977. Evolution of an active continental margin as exemplified by the Alpine history of the Caucasus. *Tectonophysics* **40**, 183–199.
- AĞAR, U. 1977. *Demirözü (Bayburt) ve Köse (Kelkit) Bölgesinin Jeolojisi [Geology of Demirözü (Bayburt) ve Köse (Kelkit) Region]*. PhD Thesis, Karadeniz Technical University, Trabzon [in Turkish with English abstract, unpublished].
- AKIN, H. 1978. Geologie, Magmatismus und Lagerstaettenbildung im ostpontischen Gebirge-Türkei aus der Sicht der Plattentektonik. *Geologische Rundschau* **68**, 253–283.
- ALTHERR, R., HOLL, A., HEGNER, E., LANGER, C. & KREUZER, H. 2000. High potassium, calc-alkaline I-type plutonism in the European Variscides: northern Vosges (France) and northern Schwarzwald (Germany). *Lithos* **50**, 51–73.
- ALTHERR, R. & SIEBEL, W. 2002. I-type plutonism in a continental back-arc setting: Miocene granitoids and monzonites from the central Aegean Sea, Greece. *Contributions to Mineralogy and Petrology* **143**, 397–415.
- ANDERSON, J.L. & SMITH, D.R. 1995. The effects of temperature and oxygen fugacity on the Al-in-hornblende barometry. *American Mineralogist* **80**, 549–559.
- ARSLAN, M. & ASLAN, Z. 2005. Mineralogy, petrography and whole-rock geochemistry of the Tertiary granitic intrusions in the Eastern Pontides, Turkey. *Journal of Asian Earth Sciences* **27**, 177–193.
- ARSLAN, M., TÜYSÜZ, N., KORKMAZ, S. & KURT, H. 1997. Geochemistry and petrogenesis of the eastern Pontide volcanic rocks, Northeast Turkey. *Chemie der Erde* **57**, 157–187.
- ARSLAN, M., ASLAN, Z. & ŞEN, C. 1999. Post-collision granitic intrusions of Eastern Pontides, NE Turkey: implications to Pontide arc evolution during Tertiary time. In: BARBARIN, B. (ed), *The Origin of Granites and Related Rocks*. 4th Hutton Symposium, p. 124.
- ARSLAN, M., ŞEN, C., ALİYAZİCİOĞLU, İ., KAYGUSUZ, A. & ASLAN, Z. 2000. Trabzon ve Gümüşhane yörelerinde (KD, Türkiye) yüzeylenen Eosen (?) volkanitlerinin karşılaştırmalı jeolojisi, mineralojisi ve petrolojisi [Comparative geology, mineralogy and petrology of Eocene (?) volcanics in Trabzon and Gümüşhane areas (NE, Turkey)]. *Yerbilimleri ve Madencilik Kongresi Bildiriler Kitabı* **1**, 39–53 [in Turkish with English abstract].
- ARSLAN, M., KOLAYLI, H. & TEMİZEL, İ. 2004. Petrographical, geochemical and petrological characteristics of the Güre (Giresun, NE Turkey) Granitoid. *Bulletin of Earth Sciences Application and Research Centre of Hacettepe University* **30**, 1–21.
- BACON, C.R. & DRUITT, T.H. 1988. Compositional evolution of the zoned calc-alkaline magma chamber of Mount Mazama, Crater Lake, Oregon. *Contributions to Mineralogy and Petrology* **98**, 224–256.
- BARBARIN, B. 1988. Field evidence for successive mixing and mingling between the Piolard Diorite and the Saint-Julien-La-Vêtre Monzogranite (Nord-Forez, Massif Central, France). *Canadian Journal of Earth Sciences* **25**, 49–59.
- BARBARIN, B. 1999. A review of the relationships between granitoid types, their origins and their geodynamic environments. *Lithos* **46**, 605–626.
- BAXTER, S. & FEELY, M. 2002. Magma mixing and mingling textures in granitoids: examples from the Galway Granite, Ireland. *Mineralogy and Petrology* **76**, 63–74.
- BEARD, J.S., LOFGREN, G.E., SINKA, A.K. & TOLLO, R.P. 1994. Partial melting of apatite-bearing charnockite, granulite, and diorite: melt compositions, restite mineralogy, and petrologic implications. *Journal of Geophysical Research* **99**, 21591–21604.
- BEKİTAŞ, O. & ÇAPKINOĞLU, Ş. 1997. Neptunian dikes and block tectonics in the eastern Pontide Magmatic Arc, NE Turkey: implications for the kinematics of the Mesozoic basins. *Geosound* **30**, 451–461.
- BLUNDY, J.D. & HOLLAND, T.J.B. 1990. Calcic amphibole equilibria and a new amphibole-plagioclase geothermometer. *Contributions to Mineralogy and Petrology* **104**, 208–224.
- BOZTUĞ, D. 2008. Petrogenesis of the Kösedağ Pluton, Suşehri-NE Sivas, east-central Pontides, Turkey. *Turkish Journal of Earth Sciences* **17**, 241–262.
- BOZTUĞ, D., ERÇİN, A.İ., KURUCELİK, M.K., Göç, D., KÖMÜR, İ. & İSKENDERİOĞLU, A. 2006. Geochemical characteristics of the composite Kaçkar batholith generated in a Neo-Tethyan convergence system, Eastern Pontides, Turkey. *Journal of Asian Earth Sciences* **27**, 286–302.
- BOZTUĞ, D., JONCKHEERE, R., WAGNER, G.A. & YEĞİNGİL, Z. 2004. Slow Senonian and fast Palaeocene-Early Eocene uplift of the granitoids in the Central Eastern Pontides, Turkey: apatite fission-track results. *Tectonophysics* **382**, 213–228.

- BOZTUĞ, D., KUŞÇU, İ., ERÇİN, A.İ., AVCI, N. & ŞAHİN, S.Y. 2003. Mineral deposits associated with the pre-, syn- and post-collisional granitoids of the Neo-Tethyan convergence system between the Eurasian and Anatolian plates in NE and Central Turkey. In: ELIOPoulos, D. et al. (eds) *Mineral Exploration and Sustainable Development*. Millpress, Rotterdam, 1141–1144.
- BROWN, G.C., THORPE, R.S. & WEBB, P.C. 1984. The geochemical characteristics of granitoids in contrasting arcs and comments on magma sources. *Journal of the Geological Society, London* **141**, 413–426.
- ÇAMUR, M.Z., GÜVEN, İ.H. & ER, M. 1996. Geochemical characteristics of the Eastern Pontide volcanics: An example of multiple volcanic cycles in arc evolution. *Turkish Journal of Earth Sciences* **5**, 123–144.
- CHAPPELL, B.W. & WHITE, A.J.R. 1974. Two contrasting granite types. *Pacific Geology* **8**, 173–174.
- CHAPPELL, B.W. & WHITE, A.J.R. 1992. I- and S-type granites in the Lachlan Fold Belt. *Transactions of the Royal Society of Edinburgh: Earth Sciences* **83**, 1–26.
- CRAWFORD, M.B. & SEARLE, M.P. 1992. Field relationships and geochemistry of precollisional (India–Asia) granitoid magmatism in the central Karakoram, northern Pakistan. *Tectonophysics* **206**, 171–192.
- ÇOĞULU, E. 1975. *Gümüşhane ve Rize Granitik Plutonlarının Mukayeseli Petrojeolojik ve Jeokronolojik Etüdü [Petrogeologic and Geochronologic Investigation of Gümüşhane and Rize Granitic Plutons and Their Comparison]*. Dissertation Thesis, İstanbul Technical University [in Turkish with English abstract, unpublished].
- DEBON, F. & LE FORT, P. 1982. A chemical-mineralogical classification of common plutonic rocks and associations. *Transactions of the Royal Society of Edinburgh: Earth Sciences* **73**, 135–149.
- DEBON, F., LE FORT, P., DAUTEL, D., SONET, J. & ZIMMERMANN, J.L. 1987. Granites of western Karakoram and northern Kohistan (Pakistan): a composite Mid-Cretaceous to Upper Cenozoic magmatism. *Lithos* **20**, 19–40.
- DELALOYE, M., ÇOĞULU, E. & CHESSEX, R. 1972. Etude géochronométrique des massifs cristallins de Rize et de Gümüşhane, Pontides Orientales (Turquie). *Archives des Sciences Physiques et Naturelles* **25**, Supplement 7, 43–52.
- DEPAOLO, D.J. 1981. Trace element and isotopic effects of combined wallrock assimilation and fractional crystallization. *Earth and Planetary Science Letters* **53**, 189–202.
- DOKUZ, A., TANYOLU, E. & GENÇ, S. 2006. A mantle- and a lower crust-derived bimodal suite in the Yusufeli (Artvin) area, NE Turkey: trace element and REE evidence for subduction-related rift origin of Early Jurassic Demirkent intrusive complex. *International Journal of Earth Sciences* **95**, 370–394.
- DRUMMOND, M.S. & DEFANT, M.J. 1990. A model for trondhjemite-tonalite-dacite genesis and crustal growth via slab melting: Archean to modern comparisons. *Journal of Geophysical Research* **95**, 21503–21521.
- EĞİN, D., HIRST, D.M. & PHILLIPS, R. 1979. The petrology and geochemistry of volcanic rocks from the northern Harşit river area, Pontide volcanic province, northeast Turkey. *Journal of Volcanology and Geothermal Research* **6**, 105–123.
- EYÜBOĞLU, Y., BEKTAS, O. & PUL, D. 2007. Mid-Cretaceous olistostromal ophiolitic melange developed in the back-arc basin of the eastern Pontide magmatic arc, northeast Turkey. *International Geology Review* **49**, 1103–1126.
- FLOYD, P.A. & WINCHESTER, J.A. 1975. Magma type and tectonic setting discrimination using immobile elements. *Earth and Planetary Science Letters* **27**, 211–218.
- FROST, B.R., BARNES, C.G., COLLINS, W.J., ARCALUS, R.J., ELLIS, D.J. & FROST, C.D. 2001. A geochemical classification for granitic rocks. *Journal of Petrology* **42**, 2033–2048.
- GALAN, G., PIN, C. & DUTHON, J.L. 1996. Sr–Nd isotopic record of multi-stage interactions between mantle derived magmas and crustal components in a collision context: the ultramafic-granitoid association from Vivero (Hercynian belt, NW Spain). *Chemical Geology* **131**, 67–91.
- GARDIEN, V., THOMPSON, A.B., GRUJIC, D. & ULMER, P. 1995. Experimental melting of biotite + plagioclase + quartz ± muscovite assemblages and implications for crustal melting. *Journal of Geophysical Research* **100**, 15581–15591.
- GEDİKOĞLU, A. 1978. *Harşit Granit Karmaşığı ve Çevre Kayaçları [Harşit Granite Complex and its Country Rocks (Giresun-Doğankent)]*. PhD Thesis, Karadeniz Technical University, Trabzon [in Turkish with English abstract, unpublished].
- GEDİK, A., ERCAN, T., KORKMAZ, S. & KARATAŞ, S. 1992. Rize-Fındıklı Çamlıhemşin arasında (Doğu Karadeniz) yer alan magmatik kayaçların petrolojisi ve Doğu Pontidlerdeki bölgesel yayılımları [Petrology of the magmatic rocks around Rize-Fındıklı-Çamlıhemşin (eastern Black Sea) and their distribution at the eastern Pontides]. *Geological Bulletin of Turkey* **35**, 15–38 [in Turkish with English abstract].
- GILES, D.L. 1974. *Geology and Mineralization of the Ulutaş Copper-molybdenum Prospect, Mineral Exploration in Two Areas*. UNDP Technical Report, 6, MTA, Ankara [unpublished].
- GÜVEN, İ.H. 1993. *1/250,000-Scale Geological and Metallogenical Map of the Eastern Black Sea Region*. Publications of Mineral Research and Exploration Institute of Turkey (MTA), Trabzon.
- HAMMASTROM, J.M. & ZEN, E.A. 1986. Aluminum in hornblende: an empirical igneous geobarometer. *American Mineralogist* **71**, 1297–1313.
- HARRIS, N.B.W., PEARCE, J.A. & TINDLE, A.G. 1986. Geochemical characteristics of collision-zone magmatism. In: COWARD, M. P. & RIES, A. C. (eds), *Collision Tectonics*. Geological Society, London, Special Publications **19**, 67–81.
- HIBBARD, M.J. 1991. Textural anatomy of twelve magma-mixed granitoid systems. In: DIDIER, J. & BARBARIN, B. (eds), *Enclaves and Granite Petrology*. Developments in Petrology, Vol 13, Elsevier, Amsterdam, 431–444.

- HOLLISTER, L.S., GRISSOM, G.C., PETERS, E.K., STOWELL, H.H. & SISSON, V.B. 1987. Confirmation of the empirical correlation of Al in hornblende with pressure of solidification of calc-alkaline plutons. *American Mineralogist* **72**, 231–239.
- İLBİYİLÜ, N. 2008. Geochemical characteristics of the Şebinkarahisar granitoids in the Eastern Pontides, northeast Turkey: Petrogenesis and tectonic implications. *International Geology Review* **50**, 563–582.
- IRVINE, T.N. & BARAGAR, W.R.A. 1971. A guide to chemical classification of the common volcanic rocks. *Canadian Journal of Earth Sciences* **8**, 523–548.
- JICA. 1986. *The Republic of Turkey Report on the Cooperative Mineral Exploration of Gümüşhane Area, Consolidated Report*. Japanese International Cooperation Agency, Metal Mining Agency of Japan.
- KARSLI, O., AYDIN, F. & SADIKLAR, M.B. 2004. Magma interaction recorded in plagioclase zoning in granitoid systems, Zigana Granitoid, Eastern Pontides, Turkey. *Turkish Journal of Earth Sciences* **13**, 287–305.
- KAYGUSUZ, A. 2000. *Torul ve Çevresinde Yüzeylenen Kayaçların Petrografik ve Jeokimyasal İncelenmesi [Petrographic and Geochemical Investigations of Rocks Exposing in and Around Torul]*. PhD Thesis, Karadeniz Technical University, Trabzon [in Turkish with English abstract, unpublished].
- KAYGUSUZ, A. & ŞEN, C. 1998. Torul (Gümüşhane) granitoyidinin petrografik ve kimyasal karakterleri [Petrographic and chemical characteristics of Torul (Gümüşhane) granitoid]. *Fırat Üniversitesi Jeoloji Mühendisliği Eğitiminin 20. Yılı Sempozyumu Bildirileri*, 381–388 [in Turkish with English abstract].
- KAYGUSUZ, A., WOLFGANG, S., ŞEN, C. & SATIR, M. 2008. Petrochemistry and petrology of I-type granitoids in an arc setting: the composite Torul pluton, Eastern Pontides, NE Turkey. *International Journal of Earth Sciences* **97**, 739–764.
- KAYGUSUZ, A. & AYDINÇAKIR, E. 2009. Mineralogy, whole-rock and Sr-Nd isotope geochemistry of mafic microgranular enclaves in Cretaceous Dagbasi granitoids, Eastern Pontides, NE Turkey: Evidence of magma mixing, mingling and chemical equilibration. *Chemie der Erde-Geochemistry* **69**, 247–277.
- KAZMIN, V.G., SBORTSHIKOV, I.M., RICOU, L.E., ZONENSHAIN, L.P., BOULIN, J. & KNIPPER, A. 1986. Volcanic belts as markers of the Mesozoic–Cenozoic evolution of Tethys. *Tectonophysics* **123**, 123–152.
- KETİN, İ. 1966. Anadolu'nun tektonik birlikleri [Tectonic units of Anatolia]. MTA Dergisi **66**, 22–34.
- KÖPRÜBAŞI, N., ŞEN, C. & KAYGUSUZ, A. 2000. Doğu Pontid adayı granitoyidlerin karşılaştırılmalı petrografik ve kimyasal özellikleri [Comparative petrographical and chemical features of the eastern Pontide arc granitoid]. *Uygulamalı Yerbilimleri* **1**, 111–120 [in Turkish with English abstract].
- KORKMAZ, S., TÜYSÜZ, N., ER, M., MUSAOĞLU, A. & KESKİN, İ. 1995. Stratigraphy of the Eastern Pontides, NE Turkey. In: ERLER, A. et al. (eds), *Proceedings of the international symposium of the geology of the Black Sea Region*, 59–69.
- LAMEYRE, J. & BOWDEN, P. 1982. Plutonic rock type series: discrimination of various granitoids series and related rocks. *Journal of Volcanology and Geothermal Research* **14**, 169–186.
- LEAKE, B.E., WOOLLEY, A.R., ARPS, C.E.S., BIRCH, W.D., GILBERT, M.C., GRICE, J.D., HAWTHORNE, F.C., KATO, A., KISCH, H.J., KRIVOVICHÉV, V.G., LINTHOUT, K., LAIRD, J., MANDARINO, J.A., MARESCH, W.V., NICKEL, E.H., ROCK, N.M.S., SCHUMACHER, J.C., SMITH, D.C., STEPHENSON, N.C.N., UNGARETTI, L., WHITTAKER, E.J.W. & YOUZHI, G. 1997. Nomenclature of amphiboles: report of the subcommittee on amphiboles of the international mineralogical association, commission on new minerals and mineral names. *American Mineralogist* **82**, 1019–1037.
- LESHER, C.E. 1990. Decoupling of chemical and isotopic exchange during magma mixing. *Nature* **344**, 235–237.
- LIEW, T.C. & HOFMANN, A.W. 1988. Precambrian crustal components, plutonic associations, plate environment of the Hercynian Fold Belt of central Europe: Indications from a Nd and Sr isotopic study. *Contributions to Mineralogy and Petrology* **98**, 129–138.
- LOPÉZ, S. & CASTRO, A. 2001. Determination of the fluid-absent solidus and supersolidus phase relationships of MORB-derived amphibolites in the range 4–14 kbar. *American Mineralogist* **86**, 1396–1403.
- LUDWIG, K.R. 2003. ISOPLOT 3.0: A Geochronological Toolkit for Microsoft Excel. Berkeley Geochronology Center, Special Publication No. 4.
- MANETTI, P., PECCERILLO, A., POLI, G. & CORSINI, F. 1983. Petrochemical constraints on the models of Cretaceous–Eocene tectonic evolution of the Eastern Pontide Chain (Turkey). *Cretaceous Research* **4**, 159–172.
- MOORE, W.J., MCKEE, E.H. & AKINCI, Ö. 1980. Chemistry and chronology of plutonic rocks in the Pontide mountains, northern Turkey. *Symposium of European Copper Deposits*, Belgrade, 209–216.
- NACHIT, H., RAZAFIMAHEFA, N., STUSSI, J.M. & CARRON, J.P. 1985. Composition chimique des biotites et typologie magmatique des granitoïdes. Comptes Rendus de l'Academie des Sciences de Paris **301**, 813–818.
- OKAY, A. & ŞAHİNTÜRK, Ö. 1997. Geology of the Eastern Pontides. In: ROBINSON, A.G. (ed), *Regional and Petroleum Geology of the Black Sea and Surrounding Region*. AAPG Memoir **68**, 291–311.
- ÖZSAYAR, T., PELİN, S. & GEDİKOĞLU, A. 1981. Doğu Pontidler'de Kretase [Cretaceous in the eastern Pontides]. *KTÜ Yer Bilimleri Dergisi* **1**, 65–14 [in Turkish with English abstract].

- PATIÑO DOUCE, A.E. 1997. Generation of metaluminous A-type granites by low-pressure melting of calc-alkaline granitoids. *Geology* **25**, 743–746.
- PATIÑO DOUCE, A.E. 1999. What do experiments tell us about the relative contributions of crust and mantle to the origin of granitic magmas? In: CASTRO, A., FERNANDEZ, C. & VIGNERESSE, J.L. (eds), *Understanding Granites: Integrating New and Classical Techniques*. Geological Society, London, Special Publications **168**, 55–75.
- PATIÑO DOUCE, A.E. & BEARD, J.S. 1996. Effects of P, f(O₂) and Mg/Fe ratio on dehydration melting of model metagreywackes. *Journal of Petrology* **37**, 999–1024.
- PATIÑO DOUCE, A.E. & JOHNSTON, A.D. 1991. Phase equilibria and melt productivity in the pelite system: implications for the origin of peraluminous granitoids and aluminous granulites. *Contributions to Mineralogy and Petrology* **107**, 202–218.
- PATIÑO DOUCE, A.E. & MCCARTHY, T.C. 1998. Melting of crustal rocks during continental collision and subduction. In: HACKER, B.R. & LIOU, J.G. (eds), *When Continents Collide: Geodynamics and Geochemistry of Ultra-high Pressure Rocks*. Kluwer, Academic Publisher, Dordrecht, 27–55.
- PEARCE, J.A., HARRIS, N.B.W. & TINDLE, A.G. 1984. Trace element discrimination diagram for the tectonic interpretation of granitic rocks. *Journal of Petrology* **25**, 956–983.
- PECCERILLO, R. & TAYLOR, S.R. 1976. Geochemistry of Eocene calc-alkaline volcanic rocks from the Kastamonu area, northern Turkey. *Contributions to Mineralogy and Petrology* **58**, 63–81.
- PETTERSON, M.G. & WINDLEY, B.F. 1985. Rb-Sr dating of the Kohistan arc Batholith in the trans-Himalayan of N. Pakistan and tectonic implications. *Earth Planetary Science Letters* **74**, 45–75.
- QIAO, G. 1988. Normalization of isotopic dilution analyses—a new program for isotope mass spectrometric analysis. *Scientia Sinica* **31**, 1263–1268.
- RAPP, R.P. 1995. Amphibole-out phase boundary in partially melted metabasalt, its control over liquid fraction and composition, and source permeability. *Journal of Geophysical Research* **100**, 15601–15610.
- RAPP, R.P. & WATSON, E.B. 1995. Dehydration melting of metabasalt at 8–32 kbar: implications for continental growth and crust-mantle recycling. *Journal of Petrology* **36**, 891–931.
- RAPP, R.P., WATSON, E.B. & MILLER, C.F. 1991. Partial melting of amphibolite eclogite and the origin of Archean trondhjemites and tonalites. *Precambrian Research* **51**, 1–25.
- ROBERTS, M.P. & CLEMENS, J.D. 1993. Origin of high-potassium, calc-alkaline, I-type granitoids. *Geology* **21**, 825–828.
- ROBINSON, A.G., BANKS, C.J., RUTHERFORD, M.M. & HIRST, J.P.P. 1995. Stratigraphic and structural development of the eastern Pontides, Turkey. *Journal of the Geological Society, London* **152**, 861–872.
- ROGERS, G. & HAWKESWORTH, C.J. 1989. A geochemical traverse across the North Chilean Andes: evidence for crust generation from the mantle-wedge. *Earth and Planetary Science Letters* **91**, 271–285.
- ROLLAND, Y., PICARD, C., PECHER, A., LAPIERRE, H., BOSCH, D. & KELLER, F. 2002. The Cretaceous Ladakh arc of NW Himalayan-slab melting and melt-mantle interaction during fast northward drift of Indian plate. *Chemical Geology* **182**, 139–178.
- RUSHMER, T. 1991. Partial melting of two amphibolites: contrasting experimental results under fluid-absent conditions. *Contributions to Mineralogy and Petrology* **107**, 41–59.
- SAJONA, F.G., MAURY, R.C., BELLON, H., COTTON, J. & DEFANT, M. 1996. High field strength element enrichment of Pliocene-Pleistocene Island Arc Basalts, Zamboanga Peninsula, western Mindanao (Philippines). *Journal of Petrology* **37**, 693–726.
- SCHMIDT, M.W. 1992. Amphibole composition in tonalite as a function of pressure: an experimental calibration of the Al-in-hornblende barometer. *Contributions to Mineralogy and Petrology* **110**, 304–310.
- SEN, C. & DUNN, T. 1994. Dehydration melting of a basaltic composition amphibolite at 1.5 and 2.0 GPa: implications for the origin of adakites. *Contributions to Mineralogy and Petrology* **117**, 394–409.
- SEN, C., ARSLAN, M. & VAN, A. 1998. Geochemical and petrological characteristics of the eastern Pontide Eocene (?) alkaline volcanic province, NE Turkey. *Turkish Journal of Earth Sciences* **7**, 231–239.
- SENGÖR, A.M.C., ÖZEREN, S., GENÇ, T. & ZOR, E. 2003. East Anatolian high plateau as a mantle-supported, north-south shortened domal structure. *Geophysical Research Letter* **30** (24), 8045. doi:10.1029/2003GL017858.
- SHAND, S.J. 1947. *Eruptive Rocks. Their Genesis, Composition, Classification and Their Relation to Ore-deposits*. 3rd edition, J Wiley Sons, New York.
- SINGH, J. & JOHANNES, W. 1996. Dehydration melting of tonalites: Part II. composition of melts and solids. *Contributions to Mineralogy and Petrology* **125**, 26–44.
- SKJERLIE, K.P. & JOHNSTON, A.D. 1996. Vapour-absent melting from 10 to 20 kbar of crustal rocks that contain multiple hydrous phases: implications for anatexis in the deep to very deep continental crust and active continental margins. *Journal of Petrology* **37**, 661–691.
- STEVENS, G., CLEMENS, J.D. & DROOP, G.T.R. 1997. Melt production during granulite facies anatexis: experimental data from ‘primitive’ metasedimentary protoliths. *Contributions to Mineralogy and Petrology* **128**, 352–370.
- STRECKEISEN, A. 1976. To each plutonic rock its proper name. *Earth Science Review* **12**, 1–33.
- SUN, S.S. & McDONOUGH, W.F. 1989. Chemical and isotope systematics of oceanic basalts; implication for mantle compositions and processes. In: SAUNDERS, A.D. & NORRY, M.J. (eds), *Magmatism in the Ocean Basins*. Geological Society, London, Special Publications **42**, 313–345.
- TANER, M.F. 1977. *Etude géologique et pétrographique de la région de Güneyce-İkizdere, située au sud de Rize (Pontides orientales, Turquie)*. PhD Thesis, Université de Genève [unpublished].

- TARNEY, J. & JONES, C.E. 1994. Trace element geochemistry of orogenic igneous rocks and crustal growth models. *Journal of the Geological Society, London* **151**, 855–868.
- TAYLOR, S.R. & MCLENNAN, S.M. 1985. *The Continental Crust: Its Composition and Evolution*. Oxford, Blackwell Publication.
- TEPPER, J.H., NELSON, B.K., BERGANTZ, G.W. & IRVING, A.J. 1993. Petrology of the Chilliwack batholith, North Cascades, Washington: generation of calc-alkaline granitoids by melting of mafic lower crust with variable fugacity. *Contributions to Mineralogy and Petrology* **113**, 333–351.
- THOMPSON, A.B. 1996. Fertility of crustal rocks during anatexis. *Transactions of the Royal Society of Edinburgh: Earth Sciences* **87**, 1–10.
- THOMPSON, A.B. & CONNOLLY, J.A.D. 1995. Melting of the continental crust: some thermal and petrological constraints on anatexis in continental collision zones and other tectonic settings. *Journal of Geophysical Research* **100**, 15565–15579.
- TOKEL, S. 1977. Doğu Karadeniz Bölgesi'nde Eosen yaşlı kalk alkalen andezitler ve jeotektonizma [Eocene calc-alkaline andesites and geotectonism in the Eastern Black Sea region]. *Türkiye Jeoloji Kurumu Bülteni* **20**, 49–54.
- TOPUZ, G. 2002. Retrograde P-T path of anatetic migmatites from the Pulur Massif, Eastern Pontides, NE Turkey: petrological and microtextural constraints. *First International Symposium of the Faculty of Mines (ITU) on Earth Sciences and Engineering Abstracts*, İstanbul, Turkey 2002, p. 110.
- TOPUZ, G., ALTHER, R., SCHWARZ, W.H., SIEBEL, W., SATIR, M. & DOKUZ, A. 2005. Post-collisional plutonism with adakite-like signatures: the Eocene Saraycık granodiorite (Eastern Pontides, Turkey). *Contributions to Mineralogy and Petrology* **150**, 441–455.
- VIELZEUF, D. & HOLLOWAY, J.R. 1988. Experimental determinations of the fluid-absent melting reactions in the pelitic system. *Contributions to Mineralogy and Petrology* **98**, 257–276.
- WHALEN, J.B., CURRIE, K.L. & CHAPPELL, B.W. 1987. A-type granites: geochemical characteristics, discrimination and petrogenesis. *Contributions to Mineralogy and Petrology* **95**, 407–419.
- WILLIAMS I.S. 1998. U-Th-Pb geochronology by ion microprobe. In: MCKIBBEN, M.A., SHANKS, W.C. & RIDLEY, W.I. (eds), *Application of Microanalytical Techniques to Understanding Mineralizing Processes. Reviews in Economic Geology* **7**, 1–35.
- WINther, K.T. 1996. An experimentally based model for the origin of tonalitic and trondhjemite melts. *Chemical Geology* **127**, 43–59.
- WOLF, M. & WYLLIE, P. 1994. Dehydration melting of solid amphibolite at 10 kb: the effect of temperature and time. *Contributions to Mineralogy and Petrology* **115**, 369–383.
- WYLLIE, P.J. & WOLF, M.B. 1993. Amphibolite dehydration-melting: sorting out the solidus. In: PRICHARD, H.M., ALABASTER, T., HARRIS, N.B.W. & NEARY, C.R. (eds), *Magmatic Processes and Plate Tectonics*. Geological Society, London, Special Publications **76**, 405–416.
- YEĞİNGİL, Z., BOZTUĞ, D., ER, M., ODDONE, M. & BIGAZZI, G. 2002. Timing of neotectonic fracturing by fission-track dating of obsidian in-filling faults in the İkizdere-Rize area, NE Black Sea region Turkey. *Terra Nova* **14**, 169–174.
- YILMAZ, A., ADAMIA, S., CHABUKIANI, A., CHKHOTUA, T., ERDOĞAN, K., TUZCU, S. & KARABIYIKOĞLU, M. 2000. Structural correlation of the southern Transcaucasus (Georgia) –eastern Pontides (Turkey). In: BOZKURT, E., WINCHESTER, J.A. & PIPER, J.D.A. (eds), *Tectonics and Magmatism in Turkey and Surrounding Area*. Geological Society, London, Special Publications **173**, 171–182.
- YILMAZ, S. & BOZTUĞ, D. 1996. Space and time relations of three plutonic phases in the Eastern Pontides, Turkey. *International Geology Review* **38**, 935–956.
- YILMAZ-ŞAHİN, S. 2005. Transition from arc- to post-collision extensional setting revealed by K-Ar dating and petrology: an example from the granitoids of the Eastern Pontide Igneous Terrane, Araklı-Trabzon, NE Turkey. *Geological Journal* **40**, 425–440.
- YILMAZ, Y. 1972. *Petrology and Structure of the Gümüşhane Granite and Surrounding Rocks, North-eastern Anatolia*. PhD Thesis, University of London [unpublished].
- YILMAZ, Y., TÜYSÜZ, O., YİĞİTBAS, E., GENÇ, Ş.C. & ŞENGÖR, A.M.C. 1997. Geology and tectonic evolution of the Pontides. In: ROBINSON, A.G. (ed), *Regional and Petroleum Geology of the Black Sea and Surrounding Region*. AAPG Memoir **68**, 183–226.
- ZHANG, H.-F., SUN, M., ZHOU, X. H., FAN, W. M. & YIN, J.F. 2002. Mesozoik Lithosphere Destruction Beneath the North China Craton: Evidence From Major, Trace Element, and Sr-Nd-Pb Isotope Studies of Fangcheng Basalts. *Contributions to Mineralogy and Petrology* **144**, 241–53.
- ZORPI, M.J., COULON, C. & ORISINI, J.B. 1991. Hybridization between felsic and mafic magmas in calc-alkaline granitoids: a case study in northern Sardinia, Italy. *Chemical Geology* **92**, 45–86.